Experimental Neurology 397 (2026) 115600

Contents lists available at ScienceDirect

Experimental Neurology

journal homepage: www.elsevier.com/locate/yexnr

Research paper

Meprin β elevates hippocampal soluble Aβ in the APP/V717I mouse model

Maximilian Keller [a], Celine Gallagher [b], Liana Marengo [a], Kira Bickenbach [c], Ulrich Schmitt [d], Mohammad Abukhalaf [e], Andreas Tholey [e], Simon Kreiselmaier [a], Christoph Becker-Pauly [c], Thomas Mittmann [b], Claus U. Pietrzik [a,*]

[a] Molecular Neurodegeneration, Institute for Pathobiochemistry, University Medical Center Mainz, Mainz, Germany
[b] Institute for Physiology, University Medical Center of the Johannes Gutenberg University, Mainz, Germany
[c] Unit for Degradomics of the Protease Web, Institute of Biochemistry, Christian-Albrechts-Universität zu Kiel, Kiel, Germany
[d] Leibniz-Institute for Resilience Research (LIR) gGmbH, Mainz, Germany
[e] Systemic Proteome Research & Bioanalytics, Institute for Experimental Medicine, Christian-Albrechts-Universität zu Kiel, Kiel, Germany

ARTICLE INFO

Keywords:
Meprin β
Alzheimers disease
Amyloid β
Proteomics
Electrophysiology

ABSTRACT

The emergence of Alzheimer's disease (AD) pathology has been the focus of multiple hypotheses, with amyloid β (Aβ) playing a central role due to its presence in both familial and sporadic AD. Therefore, a crucial aspect of AD research is understanding the generation of different Aβ species. Aβ peptides result from the proteolytic processing of Amyloid Precursor Protein (APP) by β- and γ-secretases, with BACE1 being the most prominent β-secretase. However, BACE1-overexpressing mouse models exhibit disadvantages, making them limited for AD research. Importantly, N-terminally truncated Aβ species, which constitute up to 70 % of Aβ in AD brains, are not generated by BACE1. In recent years, alternative proteases capable of cleaving APP have been identified, bridging the gap between N-terminally truncated Aβ species and BACE1-derived Aβ. Among these novel players, the metalloprotease meprin β has emerged as a risk factor in AD pathology, generating both N-terminally truncated and full-length Aβ species. Our primary objective was to develop a mouse model that more accurately resembles the pathology of AD beyond BACE1-overexpressing models, while simultaneously confirming APP cleavage of meprin β in the hippocampus and cerebral cortex. Overexpression of meprin β led to a marked increase in soluble Aβ levels, particularly in the hippocampus, indicating a higher vulnerability or elevated meprin β activity in this region compared to the cerebral cortex. Notably, this biochemical change occurred without any observable behavioral deficits, suggesting a region-specific role of meprin β in AD pathology that may extend beyond immediate functional impairment.

1. Introduction

Since the development of theories on the pathology of Alzheimer's disease (AD), various hypotheses have taken center stage. In particular, it is being discussed whether amyloid β (Aβ) is the central and primary pathological factor and whether its accumulation plays a decisive role, as it is initially present in both the rare familial form of AD and the far more common sporadic AD. The onset of pathology differs between these two forms: while mutations in APP and the γ-secretase complex lead to excessive formation of Aβ in familial AD (FAD), by altering APP processing and favoring longer aggregation-prone Aβ peptides (Li et al., 2019; Kelleher and Shen, 2017; Citron et al., 1992), the clearance of Aβ e.g. across the blood–brain barrier (BBB) is impaired in the sporadic form (Zhang et al., 2022). The outcome, however, is similar: Aβ oligomers first form in the brain parenchyma and subsequently accumulate into plaques composed of various Aβ species (Chen et al., 2017). Additionally, this accumulation presumably triggers an inflammatory response and activates the immune system (Webers et al., 2020).

Among the activation of the immune system, several factors and pathways can be triggered by Aβ oligomers through binding to various receptors. This may lead to several harmful processes, including increased production of reactive oxygen species (ROS) (Goure et al., 2014), hyperphosphorylation of tau proteins, leading to the formation of neurofibrillary tangles (NFTs) (Sengupta et al., 2016), endosomal

* Corresponding author.
E-mail addresses: kellerma@uni-mainz.de (M. Keller), cgallagh@uni-mainz.de (C. Gallagher), kbickenbach@biochem.uni-kiel.de (K. Bickenbach), ulrich.schmitt@lir-mainz.de (U. Schmitt), mohammad.abukhalaf@dkfz-heidelberg.de (M. Abukhalaf), a.tholey@iem.uni-kiel.de (A. Tholey), skreisel@students.uni-mainz.de (S. Kreiselmaier), cbeckerpauly@biochem.uni-kiel.de (C. Becker-Pauly), mittmann@uni-mainz.de (T. Mittmann), pietrzik@uni-mainz.de (C.U. Pietrzik).

https://doi.org/10.1016/j.expneurol.2025.115600
Received 8 September 2025; Received in revised form 2 December 2025; Accepted 16 December 2025
Available online 19 December 2025

transport disturbances ('traffic jams') due to overloaded autophagic degradation pathways (Zhang et al., 2021), as well as the dysregulation of the intracellular calcium balance through NMDA receptors or Aβ-induced pores in the cell membrane (Mishra et al., 2022). All factors likely play together and are inextricably linked, making the disentanglement very difficult.

Initial therapeutic approaches show that removing Aβ plaques or inhibiting their formation can have positive effects, e.g., an improvement in cognitive abilities. Unfortunately, current FDA-approved drugs cannot cure the disease but only delay its progression in the early stages (Mintun et al., 2021; Van Dyck et al., 2023).

Aβ is generated by the aberrant processing of APP via the amyloidogenic pathway. In detail, Aβ peptides are formed by the proteolytic processing of APP through the sequential action of β- and γ-secretases (Ridler, 2018). In addition to the classical 'full-length' Aβ species (Aβ1–40, Aβ1–42), numerous variants with different N-terminal modifications have been described (Sergeant et al., 2003; Dunys et al., 2018; Bayer, 2021). The exact physiological role of these N-terminally truncated Aβ species is still controversially discussed. At the same time, they have been identified as major components of extracellular amyloid deposits in the human brain (Bayer and Wirths, 2014). In fact, N-terminally truncated species account for up to 70 % of the Aβ forms detected in brain samples from patients with advanced AD (Wildburger et al., 2017; Wiltfang et al., 2001; Wirths and Zampar, 2019), which emphasizes their important role in the pathology of the disease. Many studies focus on the β-secretase BACE1, since it plays a central role in amyloidogenic APP-processing (Sims et al., 2023; Cole and Vassar, 2008). As BACE1 is not able to generate N-terminally truncated Aβ peptides, but only peptides starting at Aβ positions 1 and 11, mouse models facilitating BACE1 cleavage might not be an optimal solution to address AD pathology. The leading mouse model utilized in current AD research harbors the Swedish mutation (APP/swe - K670N/M671L), which may overlook important pathological factors, because of favored BACE1 cleavage (Armbrust et al., 2022). Therefore, focusing on APP/swe mouse models alone is not sufficient and might be partially misleading for the study of AD.

For N-truncated peptides, alternative proteases have been described, e.g., ADAMTS4 or meprin β (Bien et al., 2012; Marengo et al., 2022). These proteases fulfill numerous proteolytic functions and were recently identified as risk factors for AD (Patel et al., 2017; Matsuzaki et al., 2023). We and others have demonstrated the important role of Meprin β in Aβ generation in vitro (Bien et al., 2012; Becker-Pauly and Pietrzik, 2017) and, more recently, also in vivo (Marengo et al., 2022). We showed that the knockout (KO) of meprin β in a mouse model with the APP London mutation (APP/Ld), significantly slowed down the progression of the disease. KO mice developed typical AD symptoms at a later stage and their cognitive functions remained at the level of wild-type (wt) mice. These results emphasize that meprin β plays a role in AD pathogenesis.

Interestingly, meprin β cannot proteolytically process APP with the Swedish mutation (Thal et al., 2002). The mutation in this mouse model alters the amino acid sequence around the β cleavage site, leading to the loss of a large proportion of potential N-truncated Aβ species. Instead, this model focuses heavily on enhanced processing by BACE1, resulting in a biased representation of Aβ diversity compared to the full spectrum of Aβ in patient brains. Since we wanted to specifically investigate the function of meprin β, without influencing β-secretase cleavage, we deliberately refrained from mutating our animal model at the β cleavage site. Instead, we opted for the APP/Ld model, in which the mutation is located near the γ-cleavage site (V717I) (Tanghe et al., 2010).

To demonstrate the effects of meprin β-overexpression on amyloid β production, we specifically overexpressed meprin β in the hippocampus (HC) and cerebral cortex (Cx) - two regions that play a crucial role in Alzheimer's pathology and show the first amyloid deposits of all brain regions (Thal et al., 2002). We then analyzed soluble Aβ levels, investigated neuronal function using electrophysiological experiments, analyzed the behavior of the mice to identify a possible phenotype, and performed an N-terminomics assay to find potential novel substrates of meprin β in this mouse model.

2. Methods

2.1. Animals

hAPP[V717I] (Tanghe et al., 2010) mice (APP/Ld) were crossed with $NEX^{Cre;TG/wt}$ × $ROSA26^{Mep1b\text{-}HA}$ mice (Keller et al., 2025) ($mep\beta^{Cre;TG/wt}$), resulting in mice overexpressing meprin β in an APP/Ld background ($mep\beta^{Cre;TG/wt}$ x APP/Ld).

We utilized the NEX-Cre system to overexpress meprin β in the $mep\beta^{Cre;TG/wt}$ mouse model. Briefly, the NEX-Cre mouse line expresses Cre recombinase under the control of the NEX (Neurod6) promoter, which is specific to principal excitatory neurons in the dorsal telencephalon. Cre activity in this line begins around embryonic day 11.5 (E11.5), corresponding to the onset of early neuronal differentiation. At this stage, postmitotic pyramidal neurons in the neocortex and granule and mossy cells in the dentate gyrus begin to express Cre, allowing recombination of floxed alleles specifically in these cell types. There is no significant Cre activity in proliferating neural precursors, interneurons, oligodendrocytes, or astrocytes, ensuring that recombination is restricted to excitatory principal neurons. Therefore, meprin β overexpression is not inducible but constitutive. Because of its temporal and spatial specificity, NEX-Cre provides reliable recombination in forebrain excitatory neurons from mid-gestation through postnatal development and into adulthood (Goebbels et al., 2006). According to a study by Luo et al. (2020), using a male Cre driver and a female floxed gene carrier in Cre-Lox breeding minimizes the risk of unwanted germline recombination, which can otherwise lead to global knockout in offspring and compromise tissue specificity. We have adjusted our breeding accordingly, and the parents exhibited the corresponding mutations (male $NEX^{Cre;TG/wt}$ and female $ROSA26^{Mep1b\text{-}HA}$ mice). For experiments we predominantly used female $mep\beta^{Cre;TG/wt}$ mice.

Next, we crossed female $mep\beta^{Cre;TG/wt}$ mice with male heterozygous APP/Ld carriers, generating $mep\beta^{Cre;TG/wt}$ × APP/Ld offspring. The APP/Ld mutation occurs near the γ-secretase cleavage site, where valine at position 717 is substituted by isoleucine (V717I; Tanghe et al., 2010). APP with the London mutation expresses the human APP695 containing the familial AD–associated mutation under control of the murine Thy-1 promoter. The Thy-1 promoter drives strong, neuron-specific expression predominantly in forebrain regions such as the cortex and hippocampus, with minimal activity in glial or peripheral tissues. Expression of the transgene begins postnatally (P7–10), following the developmental activation of Thy-1, leading to robust and sustained overexpression of the mutant human APP protein in mature neurons (Hall and Roberson, 2012). Offspring inheriting APP mutations around the γ-secretase site from the mother have been reported to exhibit earlier or more pronounced memory and metabolic impairments compared to paternal inheritance. These maternal effects are thought to arise from intrauterine environmental factors and epigenetic contributions, whereas paternal transmission typically follows Mendelian inheritance with limited phenotypic impact (Yang et al., 2018; Saadi et al., 2025). As data specific to the APP/Ld model are limited, we followed the approach used in related mouse models, employing male APP/Ld mice for breeding and female APP/Ld and $mep\beta^{Cre;TG/wt}$ × APP/Ld mice for experiments.

APP/Ld, $mep\beta^{Cre;TG/wt}$ × APP/Ld and $mep\beta^{Cre;wt/wt}$ (wt) mice were maintained on a 12 h light/dark cycle with food and water ad libitum. All animal studies were conducted in compliance with European and German guidelines for the care and use of laboratory mice and were approved by the Central Animals Facility of the University of Mainz and the ethical committee on animal care and use of Rhineland-Palatine, Germany. In total 83 mice were used for this study.

2.2. Mouse brain lysates

Mice were euthanized by cervical dislocation and their brains were extracted. For Western blot experiments of APP, Nicastrin, PSEN and GFAP, brains were dissected into cortex and hippocampus. Hippocampi from three to five mice per group were pooled and homogenized in a buffer containing 320 mM sucrose, 10 mM HEPES, and 1 mM EDTA at a 1:6 (weight to volume) ratio. The homogenates were centrifuged at 18,000 ×*g* for 30 min, after which the soluble extract was removed, and the pellet was resuspended in 1 % NP-40 lysis buffer (150 mM NaCl, 50 mM Tris–OH, pH 8.0). Lysates were then centrifuged again at 18,000 ×*g* for 30 min, and the supernatants were collected for further analysis.

For Aβ analysis, hemispheres of the cerebral cortex and three to five pooled hippocampi were mechanically homogenized in 0.04 % DEA buffer (0,4 % DEA, 0.1 M NaCl) using the same ratio described above and subsequently ultracentrifuged at 120,000 ×g for 60 min (TLA120.2 rotor, Beckman Coulter). The DEA buffer-extracted supernatant (soluble fraction) was collected, while the pellet was resuspended in 800 µL of 0.01 M PBS containing 2 % SDS for further use. PBS and SDS protein extracts were either analyzed directly or stored at −80 °C until further use. All buffers were supplemented with protease (cOmplete, Roche) and phosphatase inhibitor cocktails (PhosSTOP, Roche) before use. For meprin β characterization, whole brains were lysed and DEA (insoluble) and PBS (soluble) fractions were extracted and analyzed.

2.3. Immunoprecipitation of amyloid β

Soluble fractions from mouse protein extracts were used for immunoprecipitation (IP). Magnetic Dynabeads (M-280 Sheep Anti-Mouse IgG, 11201D, Invitrogen), coated with sheep anti-mouse IgG, were activated with the monoclonal antibody (mAb) IC16 following the manufacturer's protocol (direct IP method) and subsequently added to the samples. IC16, which recognizes residues 1–16 of the human Aβ sequence, was used at a final concentration of 1:100 (Marengo et al., 2022).

For immunoprecipitation, total Aβ was extracted from soluble brain lysates by mixing each sample with concentrated detergent buffer containing 50 mM HEPES (pH 7.4), 150 mM NaCl, 0.5 % (*v*/v) Nonidet P-40, 0.05 % (*w/v*) SDS, and a protease inhibitor cocktail (Roche Applied Science), resulting in a 1× dilution. After overnight incubation at 4 °C, the samples were washed three times with 1× PBS containing 0.1 % (*w/v*) BSA, followed by a final wash in 10 mM Tris–HCl (pH 7.5).

The samples were then heated to 95 °C in 25 µL of sample buffer (0.36 M Bis–Tris, 0.16 M bicine, 1 % [*w/v*] SDS, 15 % [w/v] sucrose, and 0.0075 % [w/v] bromophenol blue), and the resulting supernatants were loaded for analysis which is further described in the "Urea-SDS-PAGE" section.

2.4. Urea SDS PAGE

Immunoprecipitated Aβ peptides from soluble fractions were separated using 1 mm 10 % polyacrylamide 8 M urea SDS gels, as previously described in Marengo et al. (2022). To distinguish Aβ40 from Aβ42, resolving gels were prepared with a final concentration of 0.3 M H_2SO_4. Peptides were then transferred onto an Immobilon-P PVDF membrane via semi-dry western blotting (Bio-Rad) at 47 mA per membrane for 30 min.

Membranes were boiled in PBS or MilliQ water for 3 min, then blocked in 5 % powdered milk in TBST (20 mM Tris, 137 mM NaCl, 0.1 % [*v*/v] Tween-20) for at least 30 min. Immunostaining was performed overnight using the IC16 antibody. Following washes in TBS-T, membranes were incubated with a fluorescent secondary anti-mouse antibody (1:5000, Sigma). Immunoreactive bands were detected using a fluorescence imager (BioRad, ChemiDoc™, Imaging System, USA).

2.5. SDS PAGE and western blotting

Samples for analysis were prepared in SDS loading buffer (4× Roti-Load, Carl Roth, Germany) and boiled at 95 °C. Protein extracts were separated by SDS-PAGE, transferred onto nitrocellulose membranes (Amersham Hybond ECL), and then blocked in 5 % (*w/v*) milk powder in TBS-T. Soluble fractions were used to detect total soluble N-APP (sAPP), using an anti-N-terminal APP antibody (22C11, MAB348, Millipore). Moreover, antibodies against the following proteins were used for detection: C-terminal APP (CT15, Sisodia et al., 1993), neosAPPβ (Armbrust et al., 2024), sAPPα (Biolegend, SIG-9320-05), amyloid β (IC16, Jäger et al., 2009), GAPDH (Invitrogen, PA1–987), α-tubulin (Invitrogen, 62204), meprin β (ThermoFisher, PA5–47474), β-actin (Sigma-Aldrich, A5060), Nicastrin (Sigma-Aldrich, N1660), PSEN1 (7H8, C-terminal), and GFAP (Synaptic Systems, 173004). All used antibodies are summarized in Table 1.

2.6. Sandwich enzyme-linked immunosorbent assay (ELISA)

Human Aβ1–40 and Aβ1–42 concentrations were determined using commercially available ELISA kits (27,717 and 27,718, IBL International, Hamburg, Germany) following the manufacturer's instructions. In brief, soluble and insoluble fractions were diluted at ratios of 1:50 and 1:200, respectively, before being added to wells coated with either anti-human Aβx–42 (44A3) or Aβx–40 (1A10) antibodies and incubated overnight at 4 °C. After washing, the wells were incubated for 1 h with HRP-conjugated anti-human Aβ1–x (82E1). Following additional washing steps, TMB solution was added as a substrate, and the reaction was stopped using 1 N H_2SO_4. Optical density (OD) values were measured at 450 nm using a microplate reader (Anthos reader 2010).

2.7. Electrophysiology

4-week-old female mice were deeply anaesthetized with 4 Vol%

Table 1
Summary of used antibodies, their target, host organism, dilution used in experiments and epitope.

Name and/or target	Host	Dilution (WB)	Epitope
IC16, Amyloid β	Monoclonal (mouse)	1:100	Amino acids (aa) 1–8 of amyloid β - N-terminal Aβ
22C11, APP (N-terminally)	Monoclonal (mouse)	1:1000	aa 66–81 of APP - N-terminal APP
CT15, APP (C-terminally)	Polyclonal (rabbit)	1:5000	aa 680–695 of APP - C-terminal APP
Neo-sAPPβ	Polyclonal (rabbit)	1:1000	Neo-epitope specific for sAPPβ + Asp generated by meprin-β cleavage between D672–A673 of APP, detecting amyloidogenic Aβ2–x processing
6E10, Aβ or sAPPα	Monoclonal (mouse)	1:1000	aa 3–8 of Aβ and sAPPα (C-terminal)
GAPDH	Polyclonal (rabbit)	1:5000	aa 126–140
DM1a, α-tubulin	Monoclonal (mouse)	1:10000	aa 1–412
β-actin	Polyclonal (rabbit)	1:1000	aa 20–33
Meprin β	Polyclonal (mouse)	1:2000	aa 21–594 (mouse)
Nicastrin	Polyclonal (rabbit)	1:3000	aa 693–709
7H8, PSEN1	Monoclonal (mouse)	1:3000	C-terminus
134B1, GFAP	Monoclonal (mouse)	1:1000	aa 391–405

isoflurane until complete loss of involuntary reflexes. Then they were quickly decapitated, the brain immediately removed and put into the ice-cold (4 °C) choline-based artificial cerebrospinal fluid (cACSF) perfused with carbogen (95 % oxygen (O_2) and 5 % carbon dioxide (CO_2)). This cASF cutting solution contained (in mM): NaCl (87), KCl (2.5), $NaH_2PO_4 + H_2O$ (1.25), choline chloride (37.5), $NaHCO_3$ (25) and D-glucose (25), $CaCl^*2H_2O$ (0.5), $MgCl_2$ (7) at a pH of 7.4. Next, the brain was placed on the stage of a vibratome (VT1200 S, Leica) in an orientation to cut horizontal brain slices with a thickness of 400 μm. Slices containing the distinctive hippocampal structures were selected and put into a storage chamber filled with normal, carbonated ACSF containing (in mM): NaCl (125), NaH_2PO_4 (1.25), KCl (2.5), $NaHCO_3$ (25), D-glucose (25), $CaCl_2^*2H_2O$ (2), $MgCl_2$ (1) and kept at room temperature. Slices rested in ACSF for at least 40 min before individual slices were transferred onto a multi-electrode array (MEA) chip of a two-chamber MEA system (MEA2100 System, Multi Channel Systems MCS GmbH), which was constantly perfused with normal ACSF at 32 °C. Each glass MEA chip consisted of 60 electrodes, each with a diameter of 30 μm and spaced with a 200 μm inter-electrode distance (60MEA200/30iR; Multi Channel Systems MCS GmbH). Each brain slice was placed to have well-positioned stimulating electrodes in the CA3 region and recording electrodes in the CA1 region of the hippocampus. A platinum grid was placed on top of the slices to stabilize their position. Slices were allowed to settle on the MEA chip for a minimum of 30 min before the recordings started. The electrophysiological simulation and recording protocols were generated and applied by Multi Channel Experimenter 2.2 software (Multi Channel Systems MCS GmbH) using a 50 kHz sampling rate and a Butterworth highpass 2.0 Order Filter with 200 Hz cut-off.

Input/output (I/O) curves of extracellular recorded field post-synaptic potentials (fEPSPs) were generated by electrical stimulation of one MEA electrode starting with a voltage pulse of 500 mV at a stimulus duration of 100 μs, then gradually increasing the pulse intensity by +500 mV until a maximum stimulation intensity of 5000 mV was reached. The duration between each voltage pulse stimulation was 40 s.

The paired-pulse protocol used a stimulation intensity that resulted in a fEPSP equal to approximately 30 % of the maximum evoked fEPSP amplitude from the input/output curve protocol. Paired-pulses had a 50 ms inter-stimulus interval.

To test the strength of synaptic long-term potentiation (LTP), fEPSPs were recorded with the same stimulus intensity selected for the paired-pulse protocol, on a slice-wise basis. Baseline stimulations for LTP were applied for 10 min, consisting of one stimulation per minute. Then, LTP was induced by applying a high-frequency stimulation (HFS) at 100 Hz for 1 s, followed by 60 min of baseline stimulations every 60 s. The level of HFS-induced LTP was analyzed by normalizing the mean amplitudes from the last 10 min of baseline recordings after HFS (50–60 min) to the mean of the amplitude of the initial 10 min baseline recordings before HFS. These data were compared to recordings against the independent control pathway that was generated by a second stimulation electrode located in the direction of the subiculum, as it cannot generate long-term plasticity changes in CA1. The Multi Channel Analyzer 2.2 (Multi Channel Systems MCS GmbH) software was used to record the peak value of each fEPSP amplitude.

Each data point (n) corresponds to one brain slice. Occasionally, multiple slices from an individual brain were examined. As all mice were biological replicates of the same sex, every slice, including those derived from the same brain, was treated as a biological replicate.

In our MEA recordings, synaptic responses were assessed along the Schaffer collateral pathway (CA3 to CA1), which is the established model for studying hippocampal LTP. To verify the specificity of synaptic potentiation and exclude network wide artifacts, a control pathway was included. In this control configuration, electrical stimulation was delivered within the CA1 region and responses were recorded in CA3. Because the axonal projections of the Schaffer collaterals are unidirectional from CA3 to CA1 pyramidal neurons, this reverse pathway (CA1 to CA3) does not represent a functional synaptic connection. Consequently, no LTP is expected to occur in this control configuration. The absence of potentiation in this pathway confirms that the LTP observed in the Schaffer collateral pathway results from specific synaptic modifications rather than nonspecific changes in network excitability or recording artifacts. Control recordings were assessed in brain slices of 4-week-old female wt mice. In total we used 6 wt (control and tested group), 4 APP/Ld and 4 APP/Ld × $mep\beta^{Cre;TG/wt}$ mice for the recordings.

All electrophysiological data were analyzed using the Multi Channel Analyzer 2.2 software, Microsoft Office Excel (Microsoft), and GraphPad Prism (GraphPad Software). Each data point represents one brain slice. At times several slices from the same brain were tested.

2.8. Morris' Water Maze (MWM)

For behavior analysis, 8-month-old mice were tested ($n = 5$ mice/group). Spatial learning and memory were assessed by the Morris' Water Maze hidden platform task performed as previously described with minor modifications (Marengo et al., 2022). Briefly, the water maze (diameter 120 cm) was filled with clear water (21–22 °C) one centimeter above the platform. Prominent symbols around the maze provided abundant extra-maze cues. The platform stayed in the same quadrant from day 1 to 4 and the mice were released from four different positions at the pool perimeter. Mice performed four trials per day on 4 consecutive days with a maximum length of 90s. Each day, the mice were released into the water from different locations outside the platform (d1 – north, south, east, west; d2 – W-*E*-S-N; d3 – S-W-N-E; d4 – E-N-W-S). If mice did not find the platform within the given time, they were guided to the platform. Mice were allowed to stay on the platform for 10 s to memorize the surrounding cues. On the fifth experimental day, a probe trial (60 s) without the platform was performed. Basal motor activity was evaluated by swimming speed (Supplementary Fig. 1). Learning was assessed by measuring the escape latency to find the platform. Memory capabilities were characterized by the number each mouse crossed the former platform location at probe trial and the latency to reach the location. To further assess the ability to memorize the location of the platform, the time spent in the right quarter of the platform was measured. For vision abilities, a visible platform task was done after the learning assessment at day 6. It consisted of three trials in a row, starting opposite to the platform that was indicated by a table tennis ball 15 cm above the platform. No mouse failed this task, showing that all tested mice were capable of seeing the cues.

A computerized video recording system registered the moving path and duration in water maze tests automatically. The hardware consisted of an IBM-type AT computer combined with a video digitizer and a CCD video camera. The software used for data acquisition and analysis was EthoVision XT® release 8.0 (Noldus Information Technology, Utrecht, the Netherlands).

2.9. N-terminomics

Samples ($n = 3$ per genotype) were processed according to TMT HUNTER workflow (Weng et al., 2019). Precipitated proteins were reconstituted in 1 mL (1 % SDS, 1× complete EDTA-free Protease Inhibitor Cocktail (Roche), 50 mM HEPES pH 8). Protein concentration was determined using Pierce BCA Protein Assay Kit (Thermo). One hundred micrograms of proteins of each sample were reduced and alkylated by mixing with 24 mM TCEP, 80 mM Chloroacetamide for 1 h at 25 °C in the dark. First cleanup was performed with SP3 beads (1:20 *w*/w protein to beads ratio) and ethanol (EtOH) added to 50 % (*v*/v) with mixing for 15 min at 25 °C to induce protein binding. Then, the supernatant was removed and beads were washed three times with 80 % EtOH. To commence with TMT labeling, beads were resuspended in 22.5 μL 6 M Guanidine hydrochloride, 30 μL 0.5 M HEPES (pH 8), and 4.5 μL 125 mM TCEP at 25 °C for 30 min. Isobaric tandem mass tags (0.8 mg TMT6plex reagents (Thermo)) were dissolved in 57 μL EtOH by

occasional vortexing for 5 min. Samples were separated with TMT6plex reagents and labeling was performed by adding a label to each beads-bound protein sample (one tag per sample) and mixing for 1.5 h at 25 °C in the dark. Labeling was stopped by adding 8 µL 8 % hydroxylamine for 30 min at 25 °C. A second cleanup was done by combining each group of samples and adding EtOH to 80 % for 15 min at 25 °C. Then, the supernatant was removed, and beads were washed three times with 80 % EtOH. Beads were spun down to remove any remaining liquid then reconstituted in 200 mM HEPES (pH 8). Digestion was performed with trypsin (1:50 enzyme to protein ratio) overnight at 37°. Ten microliters of the supernatant (corresponding to 15 µg of protein) was taken as a pre-HUNTER and the rest (HUNTER) was labeled with undecanal by adding EtOH to 40 %, 12 µL undecanal 97 % and sodium cyanoborohydride to 30 mM final concentration for 1 h at 37 °C. Labeled peptide solution was then acidified with Trifluoroacetic acid (TFA) to pH 3 and undecanal clean-up was performed using Sep-Pak tC18 Cartridges 1 cc (Waters). Conditioning and equilibration were performed with methanol and 40 % EtOH, 0.1 % TFA, respectively. Samples were added and 0.1 % TFA and flow through was collected. Collected fractions were dried in a Speedvac for 3 h then freeze-dried overnight. Desalting of the Pre-HUNTER and HUNTER samples was done with 10 µL Pierce C18 Spin Tips (Thermo) and Sep-Pak C18 Cartridges 1 cc (Waters), respectively. Eluted peptides were vacuum dried and stored at −20 °C until analysis.

Samples were resuspended in 3 % ACN with 0.1 % TFA and injected for LC–MS analysis. Chromatographic separation was performed on a Dionex U3000 nanoHPLC system equipped with an Acclaim pepmap100 C18 column (2 µm particle size, 75 µm × 500 mm) coupled online to the mass spectrometer. The eluents used were eluent A: 0.05 % FA, eluent B: 80 % ACN + 0.04 % FA. For pre-HUNTER samples, the separation was performed over a programmed 90 min run. Initial chromatographic conditions were 4 % B for 2 min followed by linear gradients from 4 % to 50 % B over 60 min, then 50 %–90 % B over 5 min, and 10 min at 90 % B. Following this, an interrun equilibration of the column was achieved by 13 min at 4 % B. For HUNTER samples, the separation was performed over a programmed 220 min run. Initial chromatographic conditions were 4 % B for 2 min followed by linear gradients from 4 % to 50 % B over 180 min, then 50 %–90 % B over 10 min, and 13 min at 90 % B. Following this, an interrun equilibration of the column was achieved by 15 min at 4 % B. A constant flow rate of 300 nL/min was employed. Wash runs were performed between each sample injection. Data acquisition following separation was performed on QExactive Plus (Thermo). Full scan MS spectra were acquired (350–1400 m/z, resolution 70,000) and subsequent data-dependent MS/MS scans were collected for the 10 or 15 most intense ions (Top10 or Top15) for pre-HUNTER and HUNTER, respectively, via HCD activation at NCE 33 (resolution 17,500). Dynamic exclusion (40 s duration) and a lock mass (445.120025) were enabled.

Raw data were analyzed against a database containing a reviewed Uniprot mouse proteome (*Mus musculus*) (17,530 sequences) and common contaminants (cRAP). The search was performed on Proteome Discoverer 2.2 using a SequestHT search engine with 10 ppm and 0.02 Da precursor and fragment ion tolerances, respectively. Digestion with Trypsin_R (semi) with a max of two missed cleavages was applied. Oxidation of methionine (15.995 Da), acetyl (42.011 Da), and TMT6plex (229.163 Da) at the peptide N-terminus was set as a dynamic modification. Carbamidomethylation (57.02146 Da) on cysteine and TMT6plex on lysine was set as a static modification. For labeling efficiency calculations, TMT6plex on lysine was set as a dynamic modification. Strict parsimony criteria have been applied, filtering peptides and proteins at 1 % FDR.

The mass spectrometry proteomics data have been deposited to the ProteomeXchange Consortium (http://proteomecentral.proteomexchange.org) via the PRIDE partner repository (Perez-Riverol et al., 2025) with the dataset identifier PXD066824.

2.10. Generation of the cleavage specificity logo

The cleavage specificity logo was generated for significant cleavage events identified through N-terminomics as described in Armbrust et al. (2025). Each amino acid between P4 and P4′ (according to Schechter-Berger nomenclature (Becker-Pauly et al., 2011)) was compared to the frequency distribution in a reference set generated from all murine proteins annotated in UniProt to calculate the percentage difference. This difference is represented by the height of the letters (using the one-letter code for amino acids with a minimum frequency of 0.06).

Colour coding is as follows: red for acidic residues, blue for basic residues, black for hydrophobic residues (including alanine and proline), and green for polar residues (including tyrosine and glycine).

2.11. Statistical analysis and illustrations

All graphs and statistical analyses were prepared using GraphPad Prism 8 software (La Jolla, CA). Western blots were quantified by densitometry analysis using ImageJ v.1.52 (NIH, USA). The individual statistical tests were described in the respective figure descriptions (ns: $p > 0.05$; *: $p \leq 0.05$; **: $p \leq 0.01$; ***: $p \leq 0.001$). The figures were created with Microsoft PowerPoint, BioRender.com and/or GraphPad.

2.12. Antibodies

See Table 1.

3. Results

3.1. Generation of the mepβCre;TG/wt × APP/Ld mouse model

To generate a novel Alzheimer's disease (AD) mouse model, we crossed mice overexpressing meprin β with mice expressing human transgenic amyloid precursor protein (APP). The APP variant carries the London mutation (APP/Ld, V717I), specifically affecting the γ-secretase cleavage site (Dewachter et al., 2000). To demonstrate the specificity of meprin β on the β-secretase cleavage side we could not use any mouse model carrying the Swedish mutation, as the Swedish mutation in APP results in a higher affinity toward BACE1 simultaneously suppressing the cleavage activity of meprin β (Schoenherr et al., 2016). This cross-breeding resulted in a new mouse model featuring neuronal overexpression of meprin β, an alternative protease for APP processing.

For targeted neuronal overexpression, we utilized the NEX-Cre mouse model previously described by Keller et al. (2025), in which Cre recombinase is expressed under the control of neuronal-specific regulatory elements from the NEX gene. The coding region (exon 2) of NEX was replaced by a Cre cassette through homologous recombination (Peters et al., 2022). These NEX-Cre mice were crossed with previously characterized meprin β knock-in mice (Peters et al., 2022). The knock-in was created by integrating murine meprin β cDNA into the STOP-EGFP-ROSA-CAG targeting vector at the Rosa26 locus in embryonic stem cells via homologous recombination (Keller et al., 2025). The resulting mice selectively overexpressed meprin β in neurons of regions critical for learning and memory, notably the hippocampus and cerebral cortex - areas first affected in AD pathology. To further confirm the functional role, we bred the meprin β-overexpressing mice into the APP/Ld (V717I) AD mouse model. This cross yielded triple-transgenic mice ($NEX^{Cre;wt/wt} \times ROSA26^{Mep1b\text{-}HA} \times hAPP[V717I]^{TG/wt}$, abbreviated as $mep\beta^{Cre;TG/wt} \times$ APP/Ld), allowing for detailed investigation of amyloidogenic pathway dynamics (Fig. 1A).

To assess the impact of meprin β overexpression on APP processing in the APP/Ld background, we performed Western blot analyses on brain lysates from APP/Ld and $mep\beta^{Cre;TG/wt} \times$ APP/Ld mice (Fig. 1B). After using antibodies that detect the APP N-terminus (22C11 – NT-APP) and C-terminus (CT15 – CT-APP) no significant differences in total soluble APP secretion or full-length APP expression between the genotypes were

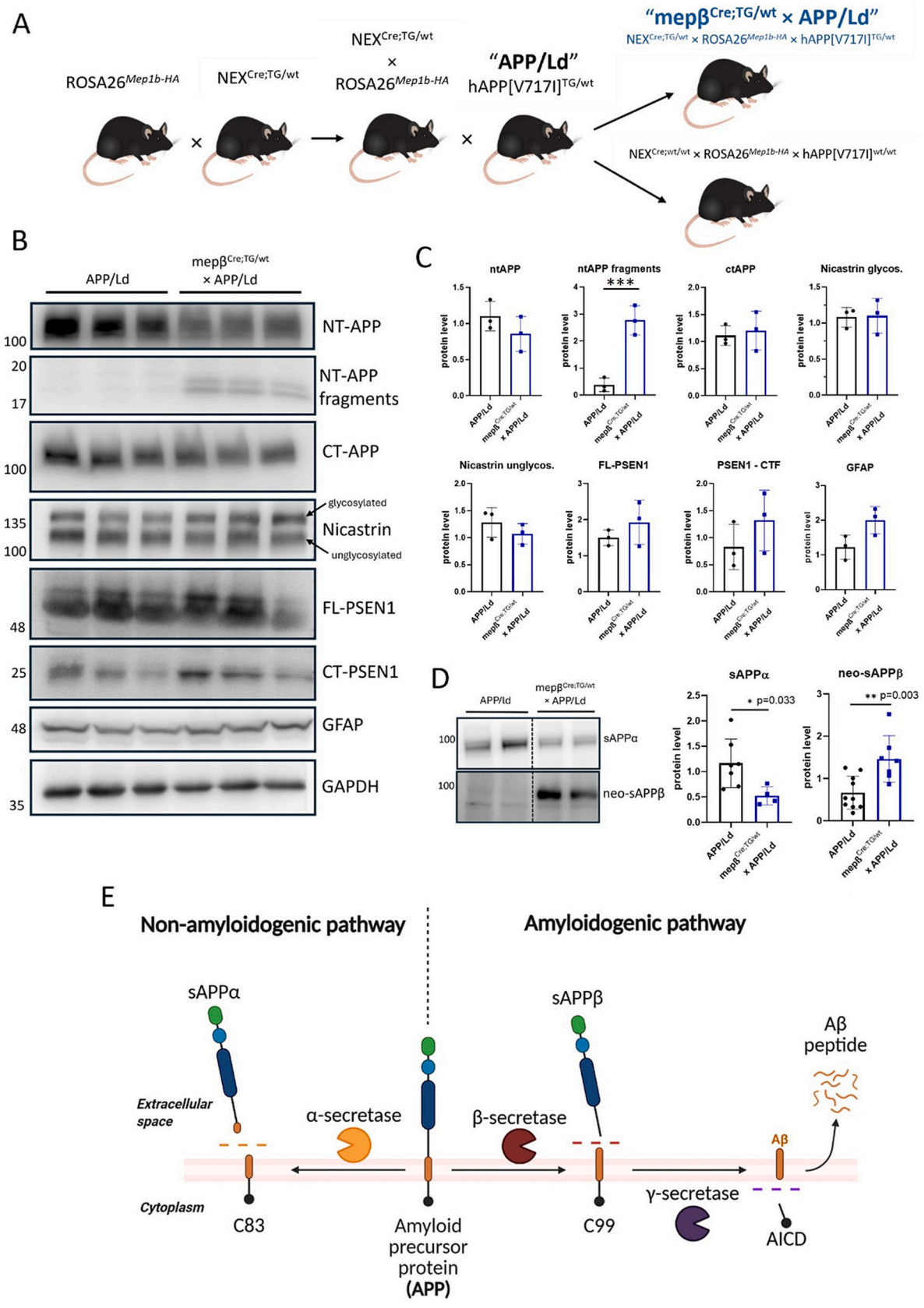

(caption on next page)

Fig. 1. Generation of a novel AD-mouse model overexpressing meprin β in cortical and hippocampal neurons. Brain lysates originated from 12-month-old female mice. (A) Homozygous transgenic ROSA26$^{Mep1b\text{-}HA}$ mice were crossed with heterozygous NEX^{Cre} mice, yielding NEX$^{Cre;TG/wt}$ × ROSA26$^{Mep1b\text{-}HA}$ (mepβ$^{Cre;TG/wt}$) offspring. Double-transgenic mepβ$^{Cre;TG/wt}$ mice were crossed with hAPP[V717I]$^{TG/wt}$ (APP/Ld) mice, resulting in the triple-transgenic novel animal model NEX$^{Cre;TG/wt}$ × ROSA26$^{Mep1b\text{-}HA}$ × hAPP[V717I]$^{TG/wt}$ (mepβ$^{Cre;TG/wt}$ × APP/Ld). (B) Comparison of APP processing, several γ-secretase subunits, and astrocyte marker GFAP in RIPA fractions of pooled cortex and hippocampus samples of APP/Ld and mepβ$^{Cre;TG/wt}$ × APP/Ld mice. Meprin β overexpression leads to no significant differences in the expression of N-terminal (NT) or full-length (FL) APP. Also, no clear differences can be observed in γ-secretase subunits Nicastrin and PSEN1. GFAP, a marker for reactive astrocytes, shows no difference between the two groups. N-terminal APP fragments appear in mice that are overexpressing meprin β, possibly products of further proteolytic cleavage of N-terminal APP. (C) Densitometric quantification of protein levels normalized to GAPDH. We used an ordinary unpaired *t*-test – NT-APP: $p = 0.2507$; NT-APP fragments: $p = 0.0024$; CT-APP: $p = 0.7154$; Nicastrin glyc.: $p = 0.9109$; Nicastrin glyc.: $p = 0.3264$; FL-PSEN1: $p = 0.3201$; PSEN-CTF: *p*-value = 0.2917; GFAP: p-value = 0.0618. Significance level: $p \geq 0.05$ = ns; $p < 0.05$ = *; $p < 0.01$ = **; $p \leq 0.001$ = ***. (D) Western blotting of APP/Ld and mepβ$^{Cre;TG/wt}$ × APP/Ld brains. Meprin β overexpression leads to significantly elevated levels of sAPPβ in brains of mepβ$^{Cre;TG/wt}$ × APP/Ld (product of the amyloidogenic pathway), whereas significantly more sAPPα is detected in APP/Ld mice (product of the non-amyloidogenic pathway). Used statistical test: ordinary t-test - sAPPα: $p = 0.0326$. sAPPβ: $p = 0.0030$. Significance level: p ≥ 0.05 = ns; p < 0.05 = *; p < 0.01 = **; p ≤ 0.001 = *** (E) Schematic depiction of the non-amyloidogenic and the amyloidogenic pathway. sAPPα is a product of the non-amyloidogenic pathway, whereas sAPPβ is a product of the amyloidogenic pathway.

observed (Fig. 1B&C). Notably, two ~18 kDa N-terminal fragments were observed specifically in mepβ$^{Cre;TG/wt}$ × APP/Ld mice, which we have previously shown to be generated by meprin β (Jefferson et al., 2013) (Fig. 1B).

To analyze potential effects of meprin β on the γ-secretase complex subunits we investigated the expression of Nicastrin and PSEN1. The levels of Nicastrin remained unchanged between groups, both in its unglycosylated ER-resident form and in its mature, glycosylated form. A non-significant trend toward increased expression of full length (FL) PSEN1, C-terminal (CT) PSEN1 and GFAP was observed in mepβ$^{Cre;TG/wt}$ × APP/Ld mice.

An increased level of Aβ peptides typically correlates with elevated sAPPβ, a cleavage product generated via the amyloidogenic pathway (Fig. 1E) (Roche et al., 2011). Since the antibody used for detection of NT-APP in Fig. 1B (22C11) does not distinguish whether APP was processed by α- or β-secretase, we next aimed to clarify the specific cleavage events. To this end, we employed the 6E10 antibody to detect sAPPα and a neosAPPβ antibody specific to APP cleavage by meprin β. As meprin β truncates Aβ N-terminally at position 2, it leaves an additional amino acid (Asp) at the C-terminus of sAPPβ, which is specifically recognized

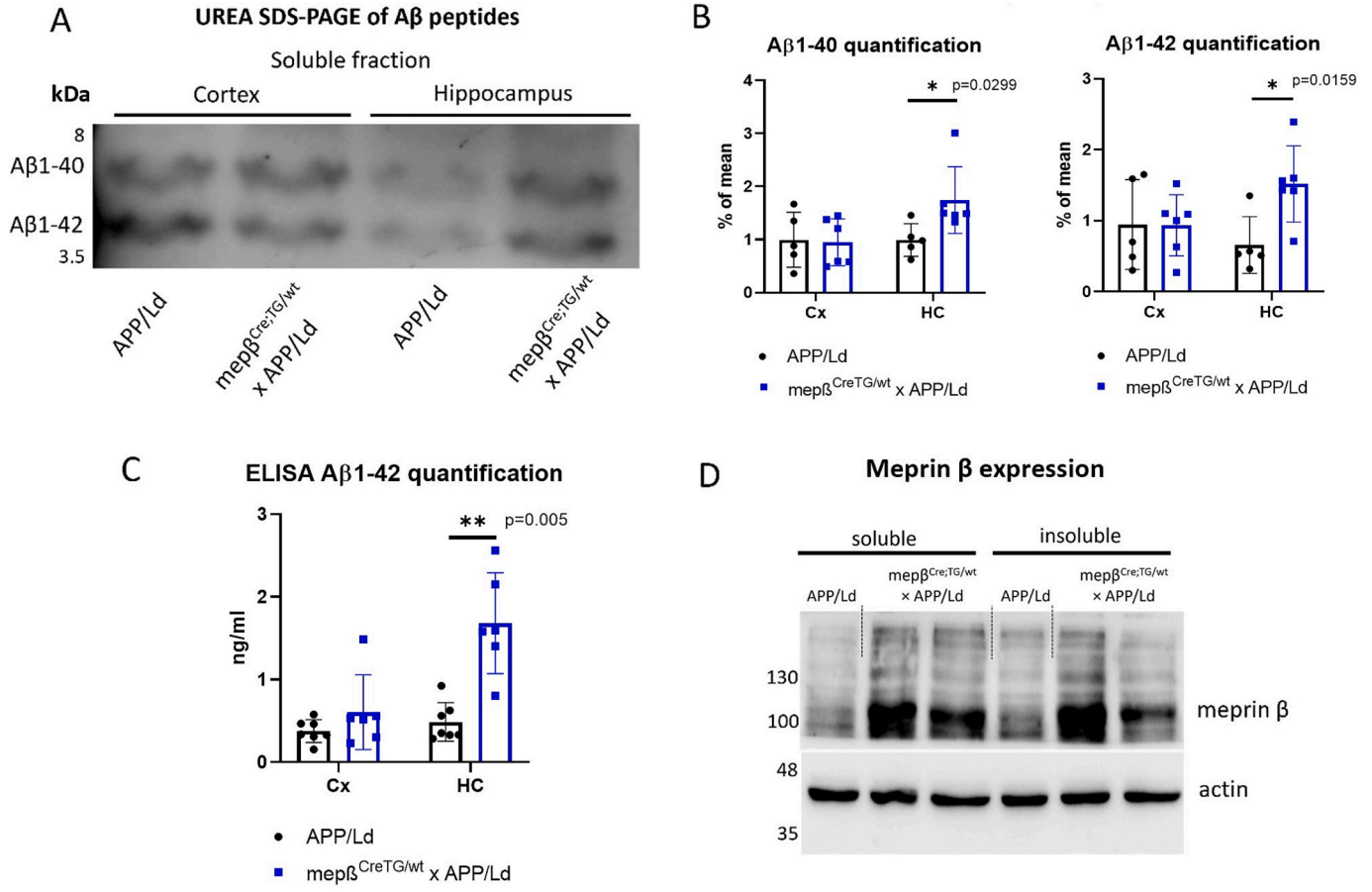

Fig. 2. Meprin β overexpression in 14-month-old female mice shows elevated levels of soluble Aβ in the hippocampus. (A) UREA SDS-PAGE and subsequent Western blotting of cortical and hippocampal brain lysates from mice show elevated levels of Aβ1–40 and Aβ1–42 in mepβ$^{Cre;TG/wt}$ × APP/Ld in the hippocampus compared to APP/Ld mice. (B) Densitometric quantification of five different biological replicates showed a significant increase in soluble Aβ1–40 and Aβ1–42 in hippocampal but not cortical neurons between mepβ$^{Cre;TG/wt}$ × APP/Ld and APP/Ld mice (unpaired t-test, Aβ1–40 Cx: $p = 0.9943$; Aβ1–40 HC: $p = 0.0299$. Aβ1–42 Cx: $p = 0.4112$; Aβ1–42 HC: $p = 0.0159$. Significance level: p ≥ 0.05 = ns; p < 0.05 = *; p < 0.01 = **; p ≤ 0.001 = ***). (C) ELISA analysis showed increased levels of Aβ1–42 (unpaired t-test, Aβ1–42 Cx: $p = 0.2978$; Aβ1–42 HC: $p = 0.0053$) in soluble fractions of mepβ$^{Cre;TG/wt}$ × APP/Ld mice compared to APP/Ld mice. (D) Western blot of meprin β expression in whole-brain lysates of APP/Ld and triple transgenic mepβ$^{Cre;TG/wt}$ × APP/Ld mice in the soluble and insoluble fractions.

by this antibody. In mice overexpressing meprin β, we observed significantly elevated levels of sAPPβ, indicating a functional role of meprin β (Fig. 1D). In contrast, APP/Ld mice exhibited significantly higher levels of sAPPα, reflecting a preferential non-amyloidogenic APP-processing (Fig. 1D). The shift toward increased sAPPβ production in meprin β-overexpressing mice demonstrate enhanced proteolytic activity of meprin β toward APP, leading to greater amyloidogenic pathway activation and higher Aβ production, as illustrated in Fig. 1E.

3.2. *Elevated Aβ 1–40/42 levels in the hippocampus of mepβCre;TG/wt × APP/Ld mice*

To evaluate the impact of meprin β overexpression in the APP/Ld mouse model, we quantified Aβ levels in the hippocampus and cerebral cortex and compared our novel mepβ$^{Cre;TG/wt}$ × APP/Ld with the APP/Ld model. Brains were isolated from female 14-month-old mice, and the hippocampus and cerebral cortex were dissected separately. Using high-speed ultracentrifugation, we separated soluble fractions from insoluble

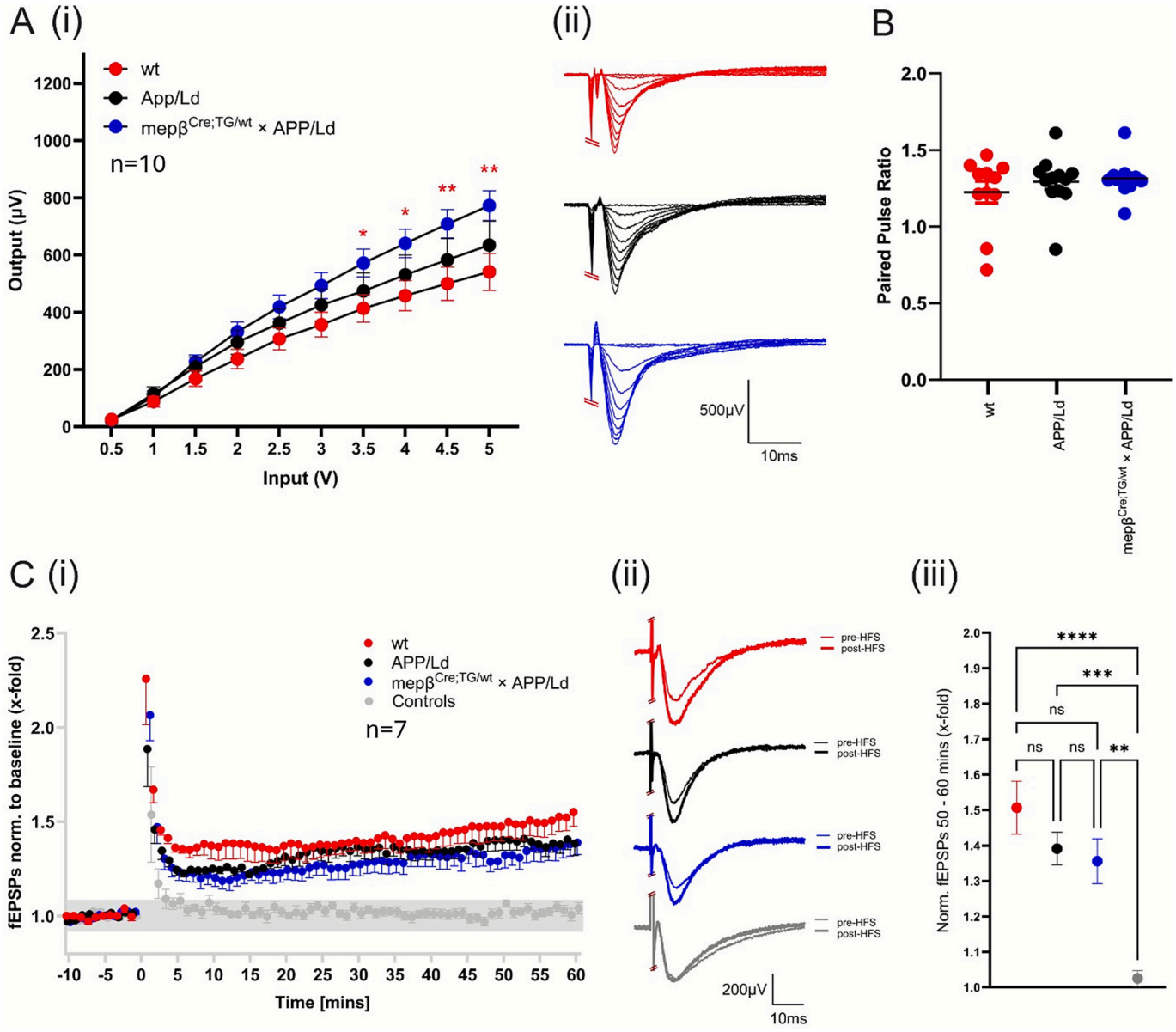

Fig. 3. 4-week-old female mepβ$^{Cre;TG/wt}$ × APP/Ld mice show increased excitability of hippocampal neurons but no change in LTP induction. (A) (i) Input/output (I/O) curves demonstrating the evoked field excitatory synaptic potential (fEPSP) amplitudes in CA1 from wildtype (red), APP/Ld (black) and mepβ$^{Cre;TG/wt}$ × APP/Ld (blue) mice. Red asterisks represent the significant difference between the wt and mepβ$^{Cre;TG/wt}$ × *APP/Ld mice.* Two-way RM ANOVA, p-value<0.0001. (ii) Representative traces of the evoked I/O fEPSPs from 0.5 to 5 V stimulations in 0.5 V-step increments. (B) Paired-pulse ratio (PPR) between the amplitude of the second and the first evoked fEPSP, with a 50 ms inter-stimulus interval, from a stimulation intensity that evoked an amplitude that is ~30 % of the maximum evoked amplitude for each slice. One-way ANOVA, p-value = 0.6244. (C) (i) Long-term potentiation (LTP) induction along the Schaffer collateral pathway using a 100 Hz high-frequency stimulation (HFS) protocol and recorded in area CA1 in wt (red), APP/Ld (black) and mepβ$^{Cre;TG/wt}$ × APP/Ld (blue) mice. Grey dots represent the recordings taken from the independent control pathway. (ii) Representative LTP fEPSP traces from wt (red), APP/Ld (black) and mepβ$^{Cre;TG/wt}$ × APP/Ld (blue) genotypes along with the traces from the independent control pathway (grey). The thinner trace of each colour shows fEPSP before the 100 Hz stimulation, while the thicker trace of each colour shows fEPSP 60 min after the tetanic stimulation. (iii) The mean relative strength of potentiation of the fEPSPs recorded at 50 to 60 min after the 100 Hz stimulation for each genotype, as well as the independent control pathway. Statistical analysis using one-way ANOVA with post-hoc Tukey's multiple comparisons test. Graphs show mean +/− S.E.M. p-value<0.0001. (For interpretation of the references to colour in this figure legend, the reader is referred to the web version of this article.)

components. Since we were interested in early disease pathology, our focus was on the soluble fraction. Insoluble components were only processed to check for membrane-bound meprin β (Fig. 2D).

Aβ levels in the soluble fraction were immunoprecipitated and analyzed using Urea SDS-PAGE, a technique suitable for detecting subtle differences in molecular weight of peptides such as Aβ1–40 and Aβ1–42. Fig. 2A provides a representative blot illustrating soluble brain lysates from APP/Ld and mepβ$^{Cre;TG/wt}$ × APP/Ld mice. In the hippocampus, we observed elevated levels of Aβ1–40/42, whereas no significant differences were detected in the cerebral cortex.

Quantitative densitometric analysis across 5 to 6 biological replicates (APP/Ld and mepβ$^{Cre;TG/wt}$ × APP/Ld groups, respectively) confirmed a significant increase in Aβ1–40/42 levels (Fig. 2B) specifically in the hippocampus. Subsequently, Aβ1–42-specific ELISA confirmed the increased soluble Aβ1–42 levels in the hippocampus, aligning with the Western blot results (Fig. 2C). Together with the shift to elevated meprin β-specific sAPPβ levels (Fig. 1C), this effect is observed likely due to meprin β's non-canonical APP cleavage. Additionally, to validate meprin β overexpression in our mouse model, we analyzed meprin β expression in whole-brain lysates prepared from combined cortical and hippocampal tissue and observed higher expression in mepβ$^{Cre;TG/wt}$ × APP/Ld compared to APP/Ld mice (Fig. 2D).

In summary, our findings demonstrate a clear effect of meprin β overexpression on Aβ levels specifically in the hippocampus. Interestingly, the cerebral cortex did not exhibit increased Aβ levels, suggesting region-specific factors influencing protease activity, potentially reflecting differences in environmental or regulatory conditions between the hippocampus and cerebral cortex in a later stage in pathology.

3.3. APP/Ld × mepβCre;TG/wt mice show increased hippocampal excitability, but no change in the strength of LTP induction

In order to clarify the possible contribution of meprin β or APP/Ld to neuronal functional alterations, we carried out electrophysiological experiments using the multielectrode array (MEA) of female 4-week-old mice. These experiments consisted of varying protocols along the Schaffer Collaterals from the hippocampal region CA3 to CA1. Basal neuronal excitability was first measured by generating an input/output curve for each genotype. Input simulations ranging from 0.5 V to 5 V and which increased in 0.5 V steps with a 40-s interstimulus interval were applied to the CA3 region. Output evoked field excitatory postsynaptic potentials (fEPSPs) were recorded in the CA1 region, where it was found that mepβ$^{Cre;TG/wt}$ × APP/Ld fEPSPs had significantly larger amplitudes at inputs 3.5–5 V when compared to wt mice but showed no differences when compared to APP/Ld fEPSPs (Fig. 3A(i)). Overlaid representative traces for each genotype can be seen in Fig. 3A(ii). Since these evoked fEPSPs mostly reflect activity from postsynaptic AMPA receptors, we also investigated potential presynaptic alterations by performing an electrical paired-pulse protocol. The stimulation intensity was decided upon on a slice-by-slice basis and equated to the stimulation intensity that produced an fEPSP amplitude that was approximately 30 % of the maximum evoked fEPSP amplitude from the input/curve protocol. The paired-pulse had a 50 ms interstimulus interval and the amplitude of the second response was divided by the amplitude of the first to generate the paired-pulse ratios (PPR) for each genotype. PPRs were comparable across all three genotypes (Fig. 3B), suggesting no major functional presynaptic alterations relative to wt mice. Finally, we wanted to elucidate any possible changes in synaptic long-term plasticity. A long-term potentiation (LTP) protocol, as a cellular model for learning and memory, was executed. Here, initial baseline fEPSPs were evoked for 10 min in the CA1 region. Next, a high-frequency stimulation (HFS) of 100 Hz with a duration of 1 s was applied to the Schaffer collaterals. Subsequently, baseline stimulation was performed for the following 60 min to disclose any potentiation of the evoked fEPSPs. The potentiation of the fEPSP amplitude for each slice was measured relative to its baseline fEPSPs and the mean was plotted for each genotype in Fig. 3C(i). The grey dots represent an independent control pathway measured in the non-potentiating direction from CA1 to CA3. Representative fEPSPs for each genotype before (thin trace) and after (thick trace) the HFS are shown in Fig. 3C(ii). All genotypes showed successful induction of LTP; however, the level of the LTP was comparable between all genotypes (Fig. 3C(iii)), indicating that the APP/Ld mutation and meprin β in mice with an APP/Ld background do not influence hippocampal LTP induction.

3.4. Mepβ$^{Cre;TG/wt}$ × APP/Ld mice show no impairment in learning and memory compared to APP/Ld mice

We aimed to compare learning and memory performance in a behavioral experiment involving three groups: mepβ$^{Cre;wt/wt}$ (wt), APP/Ld, and mepβ$^{Cre;TG/wt}$ × APP/Ld mice, using the Morris' Water Maze paradigm, where a hidden platform is submerged below the water surface, while visual cues on the tank walls help mice orientate. The mice have a certain period to find the platform, which is measured, as described in the methods section (Fig. 4A).

The mice underwent training over four consecutive days (Fig. 4B), during which no significant differences emerged among the groups. However, on the fourth training day, a measurable yet non-significant trend indicated potential differences between the wt mice and the APP/Ld and mepβ$^{Cre;TG/wt}$ × APP/Ld groups. This observed trend was consistent with the results from the probe trial day: APP/Ld mice displayed cognitive impairment compared to wt controls, while no additional impairment was detected in the mepβ$^{Cre;TG/wt}$ × APP/Ld group. Thus, the presence of the meprin β overexpression did not further exacerbate cognitive deficits.

Wt mice showed significant improvement compared to APP/Ld mice, locating the platform faster from the first to the fourth training day. Conversely, APP/Ld and mepβ$^{Cre;TG/wt}$ × APP/Ld mice showed no improvement, with the time needed to locate the platform remaining unchanged across the training days (Fig. 4B), indicating substantial learning impairment. To confirm the differences are not due to locomotion impairment, the mean swimming velocity of the mice was measured throughout the experiment, showing no differences between all groups (Supplementary Fig. 1).

During analysis, the water tank was divided into four quadrants (Fig. 4D). Throughout the training sessions, no significant differences were found in either circling behavior (grey area) or time spent across the four quadrants (Fig. 4D). In the probe trial (PT), however, wt mice exhibited a clear preference for the correct quadrant compared to the other groups (Fig. 4E). This preference highlights effective spatial learning and memory, aligning with the observed differences in escape latency (Fig. 4C&D).

In summary, transgenic mice demonstrated significant learning deficits in the Morris' Water Maze test, consistent with typical AD-related symptoms. Nonetheless, introducing meprin β-overexpression did not worsen cognitive impairment beyond that observed in APP/Ld mice.

3.5. Identification of meprin β substrates in the mepβ$^{Cre;TG/wt}$ × APP/Ld mouse model

To further investigate the causes of the electrophysiological effects, which, due to the age of the mice, are unlikely to result from AD symptoms, we performed an N-terminomics screen to identify cerebral substrates of meprin β in mepβ$^{Cre;TG/wt}$ × APP/Ld mice. We used TMT-based HUNTER analysis to compare brain lysates from mepβ$^{Cre;TG/wt}$ × APP/Ld mice and APP/Ld control mice (Fig. 5A). Through this method, we identified 5174 novel N-terminal peptides and 25 significantly altered neo N-termini when comparing brains from meprin β-overexpressing mice to APP/Ld controls (cutoff set at ±0.58 for $\log_2$ difference, $p = 0.05$) (Fig. 5B). Remarkably, two recently validated cerebral substrates of meprin β — latrophilin-3 and brevican (Armbrust

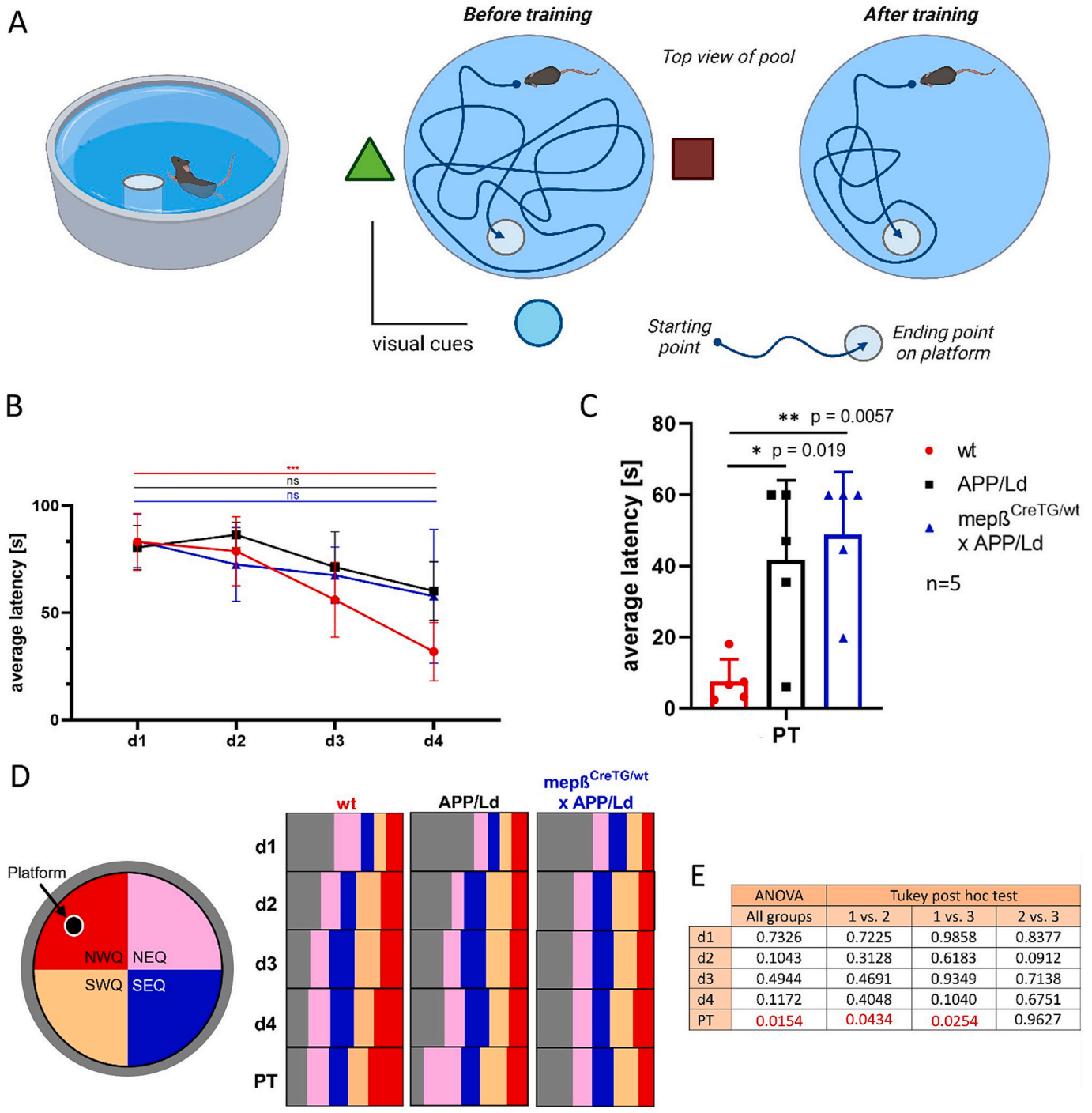

	ANOVA	Tukey post hoc test		
	All groups	1 vs. 2	1 vs. 3	2 vs. 3
d1	0.7326	0.7225	0.9858	0.8377
d2	0.1043	0.3128	0.6183	0.0912
d3	0.4944	0.4691	0.9349	0.7138
d4	0.1172	0.4048	0.1040	0.6751
PT	0.0154	0.0434	0.0254	0.9627

Fig. 4. APP/Ld mice exhibited cognitive impairment compared to wild-type controls in the Morris' water maze, but no additional deficits were observed in the mepβ$^{Cre;TG/wt}$ × APP/Ld group. Spatial learning and memory tests utilizing the Morris' water maze (MWM) paradigm were carried out on 8-month-old meprin β-overexpressing mice of mixed gender and their wt counterparts ($n = 5$). * $p < 0.05$, ** $p < 0.01$, *** $p < 0.001$ (A) Schematic overview of the Morris' Water Maze paradigm: the hidden platform is submerged below the water surface, while visual cues on the tank walls help mice orientate. Training is conducted over four days, with four trials each day. (B) Average escape latency was recorded for each trial across the four training days, but no significant differences were observed between the groups. Data shown is the mean ± SEM of four different trials performed on each day. Statistical analysis was performed using one-way ANOVA. d1: $p = 0.9136$; d2: $p = 0.3340$; d3: $p = 0.2863$; d4: $p = 0.0540$. Additionally, we compared the first and the last training day for each group to assess potential improvement using a paired t-test. Here, we could detect that only for the wt group the time to find the platform significantly decreases, whereas no difference could be observed for APP/Ld and mepβ$^{Cre;TG/wt}$ × APP/Ld (paired t-test, wt: $p = 0.0001$; APP/Ld: $p = 0.0801$. Mepβ$^{Cre;TG/wt}$ × APP/Ld: $p = 0.1004$). (C) On probe trial (PT) day, the platform was removed and the latency to reach the former platform location was measured. Significant cognitive deficits can be observed for APP/Ld and mepβ$^{Cre;TG/wt}$ × APP/Ld mice compared to wt mice. Statistical analysis was conducted applying one-way ANOVA followed by Tukey's HSD post-hoc test (one-way ANOVA, PT: $p = 0.0048$). (D&E) The water tank was divided into four equal quarters, with the platform located in the north-west quarter (NWQ). No differences were observed in time spent circling the tank (grey area) or across quadrants during training. On the PT day, significant differences emerged between wt (1) & APP/Ld (2) and wt (1) & mepβ$^{Cre;TG/wt}$ × APP/Ld (3) groups, in line with average latency results. Statistical analysis was performed using one-way ANOVA followed by Tukey's HSD post-hoc test. The table in (E) shows the *p*-values from the statistical test (one-way ANOVA for time spent in the NWQ, d1: $p = 0.7326$; d2: $p = 0.1043$; d3: $p = 0.4944$; d4: $p = 0.1172$; PT: $p = 0.0340$).

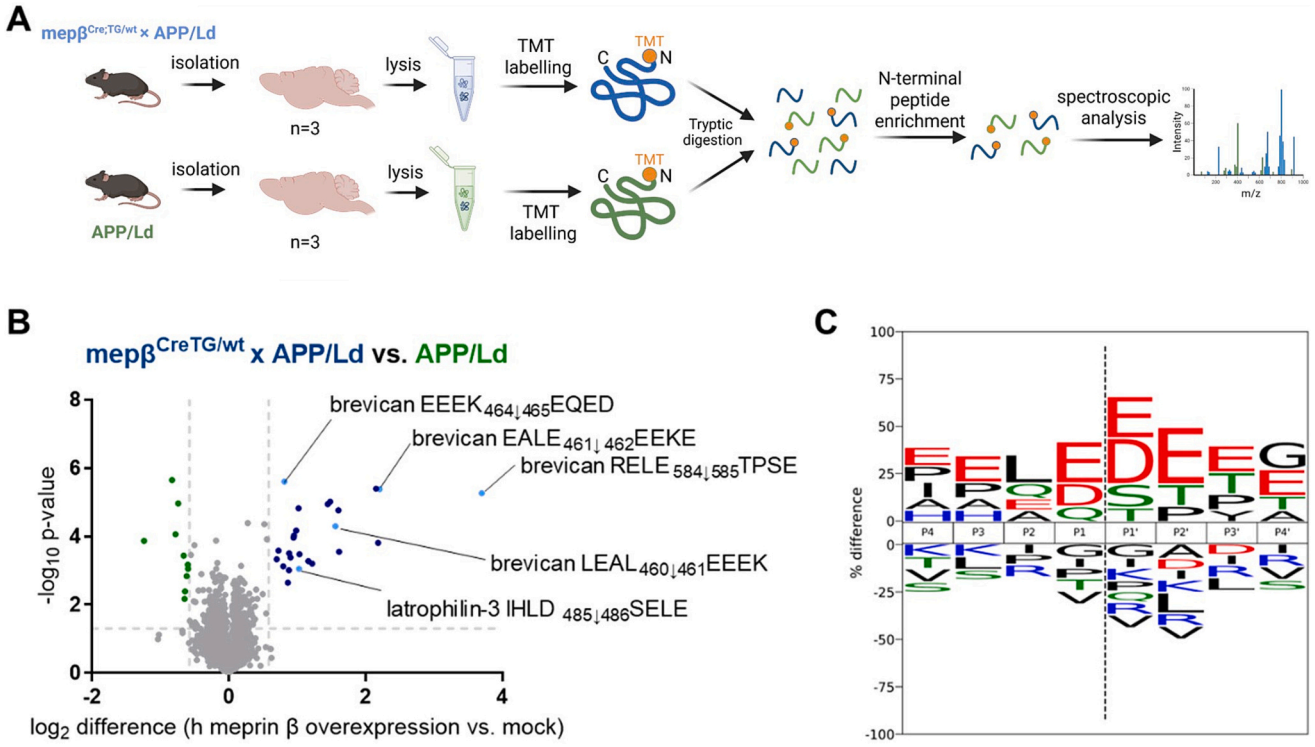

Fig. 5. Utilization of N-terminomics for the identification of substrates within the brain of mepβ$^{Cre;TG/wt}$ × APP/Ld mice. (A) Schematic overview of the TMT HUNTER-based N-terminomics approach: pooled proteins from brain lysates from female 12-month-old mepβ$^{Cre;TG/wt}$ × APP/Ld mice and APP/Ld mice ($n = 3$) were extracted and labeled with tandem mass tags (TMT) at their N-terminus. Afterwards, proteins were digested into peptides with trypsin. In a negative selection via hydrophobic tagging, internal tryptic peptides are removed to enrich the neo N-termini that are measured via mass spectrometry and quantified. (B) Volcano plots showing all identified proteolytic events detected by TMT HUNTER-based N-terminomics approach of brain lysates from mepβ$^{Cre;TG/wt}$ × APP/Ld mice compared to APP/Ld mice. Grey lines represent threshold values (±0.58 for $\log_2$ difference, p = 0.05). Selected cleavage events within known substrates are highlighted (light blue). (C) Native protein substrate cleavage specificities of meprin β calculated from significantly elevated neo N-termini in lysates from mepβ$^{Cre;TG/wt}$ × APP/Ld mice presented in specificity logos (including P4 to P4' positions). (For interpretation of the references to colour in this figure legend, the reader is referred to the web version of this article.)

et al., 2025; Keller et al., 2025) — emerged among the most prominent candidates identified in mepβ$^{Cre;TG/wt}$ × APP/Ld mice. For both substrates, cleavage sites identical or differing by only one amino acid from those found in previous N-terminomic studies were identified, reinforcing the notion of enhanced meprin β proteolytic activity specifically in mepβ$^{Cre;TG/wt}$ × APP/Ld mice. Additionally, we identified further potential substrates associated with the extracellular matrix (ECM), such as neurocan (P55066) and HAPLN1 (Q9QUR5), suggesting a possible role for meprin β in remodeling the extracellular matrix (ECM). Further confirmation arises from native substrate specificity profiling, where a cleavage specificity logo derived from significantly enriched neo N-termini demonstrates the typical specificity profile for meprin β (Becker-Pauly et al., 2011), prominently featuring acidic amino acids near the cleavage site, particularly at the P1′ position (Fig. 5C).

4. Discussion

This study aimed to investigate the role of the metalloprotease meprin β in Aβ generation using a mouse model overexpressing APP with the London (Ld) mutation, either alone or in combination with meprin β overexpression. Rather than modeling Alzheimer's disease (AD) symptoms per sé, our primary objective was to circumvent the common bias introduced by BACE1-dependent APP processing. Most conventional AD mouse models rely on the use of APPswe-based animal models that are characterized by BACE1-dependent Aβ generation (Armbrust et al., 2022), which primarily generate Aβ species starting at Aβ positions 1 and 11 (Aβ1–40/42 and Aβ11–40/42) (De Strooper et al., 2021). However, these models do not adequately reflect the diversity of N-terminally truncated Aβ variants observed in patients with sporadic AD. Since meprin β can generate such N-terminally cleaved Aβ peptides, we aimed to establish a more suitable model for studying these variants. To circumvent BACE1 biased readout, we used human APP carrying the London mutation and overexpressed murine meprin β (Keller et al., 2025). In our model the overexpression of meprin β (Mep1b) was achieved using the Cre-Lox system driven by the NEX-Cre promoter. Here, the Cre-activity begins around embryonic day 12 in newly generated glutamatergic neurons. Therefore, recombination of the floxed meprin β allele is fully established by birth (P0) (Goebbels et al., 2006). Interestingly, the murine form of meprin β is also capable of cleaving human substrates, such as APP, as demonstrated by Armbrust et al. (2024), and therefore generating Aβ peptides starting at Aβ position 1 and N-terminally truncated 2-x species. Although there are differences between human and murine meprin β, the catalytic domain remains highly conserved.

We clearly demonstrate that meprin β facilitates the proteolytic cleavage of APP, resulting in significantly elevated levels of soluble Aβ peptides in the hippocampus of meprin β-overexpressing mice in an APP/Ld background (mepβ$^{Cre;TG/wt}$ × APP/Ld) when compared to mice solely carrying the APP/Ld mutation. This increase was specific to the hippocampus and absent in the cerebral cortex. Previously, we showed that the expression of endogenous meprin β is elevated in the murine hippocampus compared to cortical areas, already paving the way for the hypothesis that meprin β activity is region-specific within the brain (Marengo et al., 2022). Other studies also showed that the activity of the γ-secretase complex is more active in the hippocampus than the cortex, which could also lead to elevated soluble Aβ in this brain region (Xiong et al., 2007; Han et al., 2021). The differences between the hippocampus and cerebral cortex may derive from regional variations in substrate

supply, co-factor expression, or overall metabolic requirements (Aldana et al., 2021; Pamplona et al., 2016; Liu et al., 2018). The concept of hippocampal vulnerability assumes that the hippocampus is particularly prone to early AD pathology due to increased excitability of neurons and lower antioxidant capacity relative to other brain regions (Duara et al., 2021; Busi et al., 2024; Jiang et al., 2020). Increased excitability of neurons was also observed in electrophysiological experiments in our study (Fig. 3A), which further supports the theory of hippocampal vulnerability in the novel mepβ$^{Cre;TG/wt}$ × APP/Ld mouse model. Moreover, other studies have shown higher levels of APP, increased metabolic stress and more pronounced synaptic decline in the hippocampus relative to others, particularly in aged or epileptic mice (Reddy et al., 2018; Aldana et al., 2021; Ostrowski et al., 2024; Van Der Kolk et al., 2005). Because the hippocampus exhibits a distinctly higher expression of soluble Aβ compared to the cerebral cortex, our study highlights this region as a uniquely susceptible site, making it an ideal target to study early molecular changes in AD.

In support of a broader role for meprin β, electrophysiological analyses revealed significant changes in synaptic excitability in 4-week-old mepβ$^{Cre;TG/wt}$ × APP/Ld mice compared to wt mice. These early effects suggest that meprin β impacts neuronal function during development, perhaps independently of Aβ. Proteomics analyses identified potential non-APP substrates, including brevican, neurocan and HAPLN1, which are involved in perineuronal net (PNN) structure, and latrophilin-3. Recent studies have further confirmed that brevican and latrophilin-3 are substrates of meprin β in the brain - the former playing a crucial role in the structural organization of PNNs (Keller et al., 2025; Armbrust et al., 2025). Its cleavage by meprin β leads to notable remodeling of the PNN. Brevican enwraps synapses and neurons, playing a crucial role in regulating neuronal plasticity (Sharma et al., 2023; Yamada et al., 1997; Sorg et al., 2016; Brakebusch et al., 2002), and likely influencing AMPA-mediated excitability in hippocampal neurons (Keller et al., 2025). Additionally, Latrophilin-3 emerged as a potential substrate in our proteomic data. It was recently confirmed as a murine meprin β substrate in astrocytes and neurons, with potential implications for cognition and links to hyperactivity (Armbrust et al., 2025). These findings extend our understanding of meprin β's activity from APP cleavage to more generalized roles in ECM remodeling and neuronal physiology. Nevertheless, studies have shown that low levels of Aβ during early brain development can have beneficial effects on synaptic growth, suggesting that the observed electrophysiological changes in the mepβ$^{Cre;TG/wt}$ × APP/Ld mice might also be attributed to the elevated Aβ concentrations (Cai et al., 2023). Additionally, Zott et al. (2019) reported that soluble Aβ oligomers impair glutamate reuptake, leading to sustained synaptic glutamate levels and hyperexcitability in neurons that are already active. This hyperactivation establishes a self-reinforcing "vicious cycle", as excessive neuronal firing further intensifies Aβ-dependent dysfunction. Importantly, these effects emerge before amyloid plaques form, implicating early glutamatergic dysregulation as a trigger of hippocampal circuit hyperexcitability. Interestingly, hyperexcitability in hippocampal neurons was observed in electrophysiological experiments conducted on 4-week-old mice, long before any AD symptoms would be expected. Additionally, the observation of early electrophysiological changes, particularly in very young mice that precede behavioral changes and may reflect synaptogenic roles of Aβ during development, raises the possibility that overexpression models may unintentionally obscure beneficial functions of Aβ by exceeding physiological levels (Cai et al., 2023). Investigating the effects of moderate Aβ elevations on developing circuits could provide new insights into both disease mechanisms and normal neurobiology.

Interestingly, despite molecular differences between APP/Ld and mepβ$^{Cre;TG/wt}$ × APP/Ld mice, no significant behavioral differences were detected in the Morris' Water Maze test. While both groups showed deficits relative to wt mice, the mepβ$^{Cre;TG/wt}$ × APP/Ld group did not display additional impairments, implying that the cognitive decline induced by APP/Ld overexpression may already saturate the measurable phenotype. This ceiling effect may obscure subtle behavioral impacts of meprin β activity and the associated increase in Aβ levels. Additionally, mice with sole meprin β overexpression also exhibit no signs of learning behavior or memory formation, further supporting the observation that a ceiling effect becomes apparent early on in this behavioral test (Keller et al., 2025).

APP/Ld mice express a mutant form of APP that promotes γ-secretase cleavage at position 42 of Aβ (Kujoth et al., 2014; Hyman et al., 2021). Generation of Aβ1–40 and Aβ1–42 peptides requires several previous cleavage steps that are separated from each other. To produce Aβ1–40 peptides, the γ-secretase sequentially cleaves at positions Aβ49, Aβ46, Aβ43 and finally at Aβ40. Similar to this sequence, Aβ1–42 is obtained by sequential cleavage at Aβ48, Aβ45 and Aβ42. This latter process is increased in the APP/Ld model, resulting in an elevated amount of Aβ42 (Steiner et al., 2018; Steiner et al., 2008; Dewachter et al., 2000). In the brains of AD patients, the Aβ1–42 to Aβ1–40 ratio is usually skewed toward Aβ1–40, with Aβ1–42 serving as the aggregation-prone core of plaques due to its increased hydrophobicity (Jenkins et al., 1996; Xu et al., 2022; Wall et al., 2016; Nguyen et al., 2016). Although our model shows a shift toward a higher Aβ1–42 proportion relative to what is commonly seen in AD patients, the Aβ1–42/Aβ1–40 ratio in our triple-transgenic mice did not differ substantially, especially when compared to highly aggressive models such as 5xFAD (Dewachter et al., 2000). Our results suggest that while meprin β increases the absolute levels of Aβ, it does not dramatically alter the peptide profile established by APP/Ld. This supports the idea that the novel mepβ$^{Cre;TG/wt}$ × APP/Ld model represents a more physiologically relevant spectrum of Aβ species, which was one of our primary objectives.

5. Conclusion

In summary, our study confirms that meprin β is a critical modulator of APP processing in vivo, selectively increasing soluble Aβ in the hippocampus. Despite this molecular alteration, we observed no exacerbation of behavioral deficits beyond those already induced by APP/Ld expression. This suggests that APP/Ld alone may suffice to model key features of AD, while overexpression of additional proteases introduces complexity without clear phenotypic gain, making it ideal to study early-pathology events of AD. However, early electrophysiological changes and proteomic signatures point to broader roles for meprin β in brain development and plasticity.

CRediT authorship contribution statement

Maximilian Keller: Writing – original draft, Visualization, Validation, Methodology, Investigation. **Celine Gallagher:** Writing – original draft, Visualization, Investigation. **Liana Marengo:** Methodology. **Kira Bickenbach:** Writing – original draft, Visualization, Data curation. **Ulrich Schmitt:** Resources. **Mohammad Abukhalaf:** Formal analysis, Data curation. **Andreas Tholey:** Writing – review & editing, Formal analysis, Data curation. **Simon Kreiselmaier:** Investigation. **Christoph Becker-Pauly:** Writing – review & editing. **Thomas Mittmann:** Writing – review & editing, Project administration. **Claus U. Pietrzik:** Writing – review & editing, Project administration, Conceptualization.

Consent for publication

All authors read and approved the final manuscript.

Ethical approval

All animal studies were conducted in compliance with European and German guidelines for the care and use of laboratory mice (EU Directive 2010/63 for the protection of animals used for scientific purposes) and were approved by the Central Animal Facility of the University of Mainz and the ethical committee on animal care and use of

Rhineland–Palatinate, Germany.

Funding

This work was supported by the Deutsche Forschungsgemeinschaft (DFG) CRC 1080 projects A15 (to CUP, CBP), C02 (to TM) and Z2 (to AT). The funding sources were not involved in study design, collection, analysis and interpretation of data, writing of the report and decision to submit the article for publication.

Declaration of competing interest

The authors declare that they have no known competing financial interests or personal relationships that could have appeared to influence the work reported in this paper.

Acknowledgements

We thank Kerstin Lüddens-Dämgen and Johanna Wesselowski for helping with everyday work in the laboratory. Also, thank you to Mona Flachsel, who helped with the MWM experiments. For the purpose of open access, the author has applied a CC-BY public copyright license to any Author Accepted Manuscript version arising from this submission.

Appendix A. Supplementary data

Supplementary data to this article can be found online at https://doi.org/10.1016/j.expneurol.2025.115600.

Data availability

All primary data and materials in the manuscript are available upon reasonable request. How to access the proteomics data is described in the supplements (only for reviewers).

References

Aldana, B., Tanila, H., Shabani, M., Westi, E., Waagepetersen, H., Andersen, J., Polli, F., Kohlmeier, K., Christensen, S., Gentry, M., Skotte, N., Mann, M., Schousboe, A., Sun, R., Freude, K., Markussen, K., Haukedal, H., Diaz-del Castillo, M., 2021. Hippocampal disruptions of synaptic and astrocyte metabolism are primary events of early amyloid pathology in the 5xFAD mouse model of Alzheimer's disease. Cell Death Dis. 12. https://doi.org/10.1038/s41419-021-04237-y.

Armbrust, F., Bickenbach, K., Marengo, L., Pietrzik, C., Becker-Pauly, C., 2022. The Swedish dilemma - the almost exclusive use of APPswe-based mouse models impedes adequate evaluation of alternative β-secretases. Biochim. Biophys. Acta, Mol. Cell Res. 1869 (3), 119164. https://doi.org/10.1016/j.bbamcr.2021.119164 (Epub 2021 Oct 23. PMID: 34699873).

Armbrust, F., Bickenbach, K., Altmeppen, H., Foggetti, A., Winkelmann, A., Wulff, P., Glatzel, M., Pietrzik, C.U., Becker-Pauly, C., 2024. A novel mouse model for N-terminal truncated Aβ2-x generation through meprin β overexpression in astrocytes. Cell. Mol. Life Sci. 81 (1), 139. https://doi.org/10.1007/s00018-024-05139-w.

Armbrust, F., Bickenbach, Kira, Koudelka, Tomas, Joos, Corentin, Keller, Maximilian, Tholey, Andreas, Pietrzik, Claus U., Becker-Pauly, Christoph, 2025. HYTANE-identified Latrophilin-3 cleavage by Meprin β leads to loss of the interaction domains. J. Proteome Res. 24 (4), 1832–1844. https://doi.org/10.1021/acs.jproteome.4c00912.

Bayer, T.A., 2021. N-truncated aβ starting at position four-biochemical features, preclinical models, and potential as drug target in Alzheimer's disease. Front. Aging Neurosci. 13, 710579. https://doi.org/10.3389/fnagi.2021.710579.

Bayer, T.A., Wirths, O., 2014. Focusing the amyloid cascade hypothesis on N-truncated Abeta peptides as drug targets against Alzheimer's disease. Acta Neuropathol. 127 (6), 787–801. https://doi.org/10.1007/s00401-014-1287-x (Epub 2014 May 7. PMID: 24803226; PMCID: PMC4024135).

Becker-Pauly, C., Pietrzik, C.U., 2017. The metalloprotease Meprin β is an alternative β-secretase of APP. Front. Mol. Neurosci. 9, 159. https://doi.org/10.3389/fnmol.2016.00159. PMID: 28105004; PMCID: PMC5215381.

Becker-Pauly, C., Barré, O., Schilling, O., Auf dem Keller, U., Ohler, A., Broder, C., Schütte, A., Kappelhoff, R., Stöcker, W., Overall, C.M., 2011. Proteomic analyses reveal an acidic prime side specificity for the astacin metalloprotease family reflected by physiological substrates. Mol. Cell. Proteomics 10 (9), M111.009233. https://doi.org/10.1074/mcp.M111.009233 (Epub 2011 Jun 21. PMID: 21693781; PMCID: PMC3186203).

Bien, J., Jefferson, T., Causević, M., Jumpertz, T., Munter, L., Multhaup, G., Weggen, S., Becker-Pauly, C., Pietrzik, C.U., 2012. The metalloprotease meprin β generates amino terminal-truncated amyloid β peptide species. J. Biol. Chem. 287 (40), 33304–33313. https://doi.org/10.1074/jbc.M112.395608 (Epub 2012 Aug 9. PMID: 22879596; PMCID: PMC3460434).

Brakebusch, Cord, Seidenbecher, Constanze I., Asztely, Fredrik, Rauch, Uwe, Matthies, Henry, Meyer, Hannelore, et al., 2002. Brevican-deficient mice display impaired hippocampal CA1 long-term potentiation but show no obvious deficits in learning and memory. Mol. Cell. Biol. 22 (21), 7417–7427. https://doi.org/10.1128/MCB.22.21.7417-7427.2002.

Busi, G., Berron, D., Baumeister, H., Mohanty, R., Misirocchi, F., Mutti, C., Zilioli, A., Westman, E., Spallazzi, M., Florindo, I., Morelli, N., Pancaldi, B., 2024. Unveiling the hippocampal subfield changes across the Alzheimer's disease continuum: a systematic review of neuroimaging studies. Brain Imaging Behav. https://doi.org/10.1007/s11682-024-00952-0 (Epub 2024 Oct 23. PMID: 39443362).

Cai, W., Li, L., Sang, S., Pan, X., Zhong, C., 2023. Physiological Roles of β-amyloid in Regulating Synaptic Function: Implications for AD Pathophysiology. Neurosci. Bull. 39 (8), 1289–1308. https://doi.org/10.1007/s12264-022-00985-9 (Epub 2022 Nov 28. PMID: 36443453; PMCID: PMC10387033).

Chen, Gf, Xu, Th., Yan, Y., et al., 2017. Amyloid beta: structure, biology and structure-based therapeutic development. Acta Pharmacol. Sin. 38, 1205–1235. https://doi.org/10.1038/aps.2017.28.

Citron, M., Oltersdorf, T., Haass, C., McConlogue, L., Hung, A., Seubert, P., Vigo-Pelfrey, C., Lieberburg, I., Selkoe, D., 1992. Mutation of the beta-amyloid precursor protein in familial Alzheimer's disease increases beta-protein production. Nature 360 (6405), 672–674.

Cole, S.L., Vassar, R., 2008. The role of amyloid precursor protein processing by BACE1, the beta-secretase, in Alzheimer disease pathophysiology. J. Biol. Chem. 283 (44), 29621–29625. https://doi.org/10.1074/jbc.R800015200 (Epub 2008 Jul 23. PMID: 18650431; PMCID: PMC2662048).

De Strooper, B., Yarenis, L., Timmers, M., Monfared, A., Albala, B., Imbimbo, B., Watanabe, N., Hampel, H., Vanmechelen, E., Willem, M., Kimura, T., Streffer, J., Voytyuk, I., Irizarry, M., Zhou, J., Hardy, J., Vassar, R., Koyama, A., Yan, R., Vergallo, A., De Vos, A., Corbo, M., Lista, S., Nisticò, R., Kramer, L., Singh, N., 2021. The β-secretase BACE1 in Alzheimer's disease. Biol. Psychiatry. https://doi.org/10.1016/j.biopsych.2020.02.001 (Epub 2020 Feb 13. PMID: 32223911; PMCID: PMC7533042).

Dewachter, I., Van Dorpe, J., Smeijers, L., Gilis, M., Kuipéri, C., Laenen, I., Caluwaerts, N., Moechars, D., Checler, F., Vanderstichele, H., Van Leuven, F., 2000. Aging increased amyloid peptide and caused amyloid plaques in brain of old APP/V717I transgenic mice by a different mechanism than mutant presenilin1. J. Neurosci. 20 (17), 6452–6458. https://doi.org/10.1523/JNEUROSCI.20-17-06452.2000. PMID: 10964951; PMCID: PMC6772965.

Duara, R., Dickson, D., Murray, M., Carter, R., DeTure, M., Asmann, Y., Lesser, E., Ertekin-Taner, N., Hinkle, K., Graff-Radford, N., Allen, M., Moloney, C., Wang, X., Carnwath, T., Serie, D., Matchett, B., Li, H., Liesinger, A., Carrasquillo, M., Tang, X., Petersen, R., Frankenhauser, I., Azu, N., Patel, T., Quicksall, Z., Crist, A., Ross, O., Labuzan, S., 2021. Transcriptomic analysis to identify genes associated with selective hippocampal vulnerability in Alzheimer's disease. Nat. Commun. https://doi.org/10.1038/s41467-021-22399-3.

Dunys, J., Valverde, A., Checler, F., 2018. Are N- and C-terminally truncated Aβ species key pathological triggers in Alzheimer's disease? J. Biol. Chem. 293 (40), 15419–15428. https://doi.org/10.1074/jbc.R118.003999 (Epub 2018 Aug 24. PMID: 30143530; PMCID: PMC6177599).

Dyck, Van, et al., 2023. Lecanemab in early Alzheimer's disease. N. Engl. J. Med. https://doi.org/10.1056/NEJMoa2212948.

Goebbels, S., Bormuth, I., Bode, U., Hermanson, O., Schwab, M., Nave, K., 2006. Genetic targeting of principal neurons in neocortex and hippocampus of NEX-Cre mice. Genesis 44. https://doi.org/10.1002/dvg.20256.

Goure, W.F., Krafft, G.A., Jerecic, J., et al., 2014. Targeting the proper amyloid-beta neuronal toxins: a path forward for Alzheimer's disease immunotherapeutics. Alz. Res. Therapy 6, 42. https://doi.org/10.1186/alzrt272.

Hall, A.M., Roberson, E.D., 2012. Mouse models of Alzheimer's disease. Brain Res. Bull. 88 (1), 3–12. https://doi.org/10.1016/j.brainresbull.2011.11.017 (Epub 2011 Nov 28. PMID: 22142973; PMCID: PMC3546481).

Han, J., Hyun, J., Park, J., Jung, S., Oh, Y., Kim, Y., Ryu, S., Kim, S., Jeong, E., Jo, D., Park, S., Jung, Y., 2021. Aberrant role of pyruvate kinase M2 in the regulation of gamma-secretase and memory deficits in Alzheimer's disease. Cell Rep. 37 (10), 110102. https://doi.org/10.1016/j.celrep.2021.110102.

Hyman, B., Frosch, M., Pei, X., Stern, M., Saqran, L., William, C., Ramani, M., 2021. Impairment of visual cortical plasticity by amyloid-beta species. Neurobiol. Dis. 154. https://doi.org/10.1016/j.nbd.2021.105344 (Epub 2021 Mar 22. PMID: 33766652; PMCID: PMC8113107).

Jäger, S., Leuchtenberger, S., Martin, A., Czirr, E., Wesselowski, J., Dieckmann, M., Waldron, E., Korth, C., Koo, E.H., Heneka, M., Weggen, S., Pietrzik, C.U., 2009. α-Secretase-mediated conversion of the amyloid precursor protein derived membrane stub C99 to C83 limits aβ generation. J. Neurochem. 111, 1369–1382. https://doi.org/10.1111/j.1471-4159.2009.06420.x.

Jefferson, T., Auf dem Keller, U., Bellac, C., Metz, V.V., Broder, C., Hedrich, J., Ohler, A., Maier, W., Magdolen, V., Sterchi, E., Bond, J.S., Jayakumar, A., Traupe, H., Chalaris, A., Rose-John, S., Pietrzik, C.U., Postina, R., Overall, C.M., Becker-Pauly, C., 2013. The substrate degradome of meprin metalloproteases reveals an unexpected proteolytic link between meprin β and ADAM10. Cell. Mol. Life Sci. 70 (2), 309–333. https://doi.org/10.1007/s00018-012-1106-2 (Epub 2012 Sep 1. PMID: 22940918; PMCID: PMC3535375).

Jenkins, N., Wang, R., Sisodia, S., Gandy, S., Copeland, N., Price, D., Yager, D., Prada, C., Lee, M., Seekins, S., Ratovitsky, T., Thinakaran, G., Levey, A., Younkin, S., Borchelt, D., Davenport, F., Seeger, M., Eckman, C., Kim, G., Slunt, H., 1996.

Familial Alzheimer's disease–linked presenilin 1 variants elevate Aβ1–42/1–40 ratio in vitro and in vivo. Neuron 17. https://doi.org/10.1016/S0896-6273(00)80230-5.
Jiang, J., Sachdev, P., Koch, F., Thalamuthu, A., Wen, W., Mather, K., Foo, H., 2020. Associations between Alzheimer's disease polygenic risk scores and hippocampal subfield volumes in 17,161 UK biobank participants. Neurobiol. Aging 98. https://doi.org/10.1016/j.neurobiolaging.2020.11.002.
Kelleher, R., Shen, J., 2017. Presenilin-1 mutations and Alzheimer's disease. Proc. Natl. Acad. Sci. 114, 629–631. https://doi.org/10.1073/pnas.1619574114.
Keller, M., Gallagher, C., Kreiselmaier, S., Bickenbach, K., Schmitt, U., Marengo, L., Taghikhah, D., Abukhalaf, M., Tholey, A., Becker-Pauly, C., Mittmann, T., Pietrzik, C.U., 2025. Meprin β modulates brevican proteolysis impairing neural plasticity and memory formation. FASEB J. 39, e70616. https://doi.org/10.1096/fj.202500017R.
Kujoth, G., Kukreja, L., Prolla, T., Van Leuven, F., Vassar, R., 2014. Increased mtDNA mutations with aging promotes amyloid accumulation and brain atrophy in the APP/Ld transgenic mouse model of Alzheimer's disease. Mol. Neurodegener. 9. https://doi.org/10.1186/1750-1326-9-16.
Li, N., Liu, K., Qiu, Y., Zhang, H., Nakanishi, H., Qing, H., 2019. Mutations of beta-amyloid precursor protein alter the consequence of Alzheimer's disease pathogenesis. Neural Regen. Res. 14, 658–665. https://doi.org/10.4103/1673-5374.247469.
Liu, Z., Choi, W., Maletić-Savatić, M., Semerci, F., Tosun, M., Jeong, H., Karakas, C., 2018. Metabolomics of mammalian brain reveals regional differences. BMC Syst. Biol. 12. https://doi.org/10.1186/s12918-018-0644-0 (PMID: 30577853; PMCID: PMC6302375).
Luo, L., Ambrozkiewicz, M., Benseler, F., Kawabe, H., Craig, A., 2020. Optimizing nervous system-specific gene targeting with Cre driver lines: prevalence of germline recombination and influencing factors. Neuron 106, 37–65.e5. https://doi.org/10.1016/j.neuron.2020.01.008.
Marengo, L., Armbrust, F., Schoenherr, C., Storck, S.E., Schmitt, U., Zampar, S., Wirths, O., Altmeppen, H., Glatzel, M., Kaether, C., Weggen, S., Becker-Pauly, C., Pietrzik, C.U., 2022. Meprin β knockout reduces brain aβ levels and rescues learning and memory impairments in the APP/lon mouse model for Alzheimer's disease. Cell. Mol. Life Sci. 79 (3), 168. https://doi.org/10.1007/s00018-022-04205-5. PMID: 35235058; PMCID: PMC8891209.
Matsuzaki, M., Yokoyama, M., Yoshizawa, Y., et al., 2023. ADAMTS4 is involved in the production of the Alzheimer disease amyloid biomarker APP669-711. Mol. Psychiatry 28, 1802–1812.
Mintun, M.A., Lo, A.C., Duggan Evans, C., Wessels, A.M., Ardayfio, P.A., Andersen, S.W., Shcherbinin, S., Sparks, J., Sims, J.R., Brys, M., Apostolova, L.G., Salloway, S.P., Skovronsky, D.M., 2021. Donanemab in early Alzheimer's disease. N. Engl. J. Med. 384 (18), 1691–1704. https://doi.org/10.1056/NEJMoa2100708 (Epub 2021 Mar 13. PMID: 33720637).
Mishra, S., Knupp, A., Szabo, M.P., Williams, C.A., Kinoshita, C., Hailey, D.W., Wang, Y., Andersen, O.M., Young, J.E., 2022. The Alzheimer's gene SORL1 is a regulator of endosomal traffic and recycling in human neurons. Cell. Mol. Life Sci. 79 (3), 162. https://doi.org/10.1007/s00018-022-04182-9.
Nguyen, P., Chen, Y., Lan, P., Truong, P., Li, M., Nguyen, H., Man, V., Thu, T., Tu, L., 2016. Aβ41 aggregates more like Aβ40 than like Aβ42: in silico and in vitro study. J. Phys. Chem. B 120, 30. https://doi.org/10.1021/acs.jpcb.6b06368 (Epub 2016 Jul 21. PMID: 27388669).
Ostrowski, D., Ramsey, J., Ostrowski, T., Han, B., Chimienti, K., Schodl, T., 2024. Synaptic profile and oxidative stress associated with amyloid-β in the Hippocampus. Physiology. https://doi.org/10.1152/physiol.2024.39.S1.2465.
Pamplona, R., Domínguez-González, M., Piñol-Ripoll, G., Portero-Otín, M., Ferrer, I., Berdún, R., Gil-Villar, M., Cabré, R., Mota-Martorell, N., Jové, M., Naudí, A., Ayala, V., Òbis, È., 2016. Specific metabolomics adaptations define a differential regional vulnerability in the adult human cerebral cortex. Front. Mol. Neurosci. 9. https://doi.org/10.3389/fnmol.2016.00138 (PMID: 28008307; PMCID: PMC5143679).
Patel, Tulsi, Brookes, Keeley-Joanne, Turton, James, Chaudhury, Sultan, Guetta-Baranes, Tamar, Guerreiro, Rita, Bras, Jose, Hernandez, Dena, Singleton, Andrew, Francis, Paul, Hardy, John, Morgan, Kevin, 2017. Whole-exome sequencing of the BDR cohort: evidence to support the role of the PILRA gene in Alzheimer's disease. Neuropathol. Appl. Neurobiol. 44. https://doi.org/10.1111/nan.12452.
Perez-Riverol, Y., Bandla, C., Kundu, D.J., Kamatchinathan, S., Bai, J., Hewapathirana, S., John, N.S., Prakash, A., Walzer, M., Wang, S., Vizcaíno, J.A., 2025. The PRIDE database at 20 years: 2025 update. Nucleic Acids Res. 53 (D1), D543–D553. https://doi.org/10.1093/nar/gkae1011.
Peters, F., Rahn, S., Mengel, M., Scharfenberg, F., Otte, A., Koudelka, T., Wagner, E.F., Wunderlich, F. Thomas, Haase, M., Naumann, R., Tholey, A., Becker-Pauly, C., 2022. Syndecan-1 shedding by meprin β impairs keratinocyte adhesion and differentiation in hyperkeratosis, Matrix Biology, Volume 102, 2021, Pages 37–69, ISSN 0945-053X, doi: 10.1016/j.matbio.2021.08.002. Epub 2021 Sep 8. Erratum in: Matrix Biol 105, 144. https://doi.org/10.1016/j.matbio.2021.10.003 (PMID: 34508852).
Reddy, P., Kandimalla, R., Yin, X., Mańczak, M., 2018. Hippocampal mutant APP and amyloid beta-induced cognitive decline, dendritic spine loss, defective autophagy, mitophagy and mitochondrial abnormalities in a mouse model of Alzheimer's disease. Hum. Mol. Genet. 27. https://doi.org/10.1093/hmg/ddad147 (PMID: 29408999; PMCID: PMC6455948).
Ridler, C., 2018. BACE1 inhibitors block new Aβ plaque formation. Nat. Rev. Neurol. 14, 126. https://doi.org/10.1038/nrneurol.2018.12.
Roche, S., Bennys, K., Croisile, B., Tiers, L., Lehmann, S., Gabelle, A., Quadrio, I., Gor, B., Labauge, P., Chaulet, C., Perret-Liaudet, A., Touchon, J., Vighetto, A., Tholance, Y., Geny, C., Krolak-Salmon, P., 2011. Correlations between soluble α/β forms of amyloid precursor protein and Aβ38, 40, and 42 in human cerebrospinal fluid. Brain Res. 1357. https://doi.org/10.1016/j.brainres.2010.08.022 (Epub 2010 Aug 14. PMID: 20713025).
Saadi, F., Katritch, I.V., Parhizkar, S., Lugo, B., Cho, Y., Ulrich, J.D., Holtzman, D.M., 2025. Maternal inheritance suppresses CAA and amyloid plaques in 5xFAD (Tg7031)/APOE4 mice. Neuron 113 (18), 2883–2884. https://doi.org/10.1016/j.neuron.2025.08.008.
Schoenherr, C., Bien, J., Isbert, S., et al., 2016. Generation of aggregation prone N-terminally truncated amyloid β peptides by meprin β depends on the sequence specificity at the cleavage site. Mol. Neurodegener. 11, 19. https://doi.org/10.1186/s13024-016-0084-5.
Sengupta, U., Nilson, A.N., Kayed, R., 2016. The Role of Amyloid-β Oligomers in Toxicity, Propagation, and Immunotherapy. EBioMedicine 6, 42–49. https://doi.org/10.1016/j.ebiom.2016.03.035 (Epub 2016 Apr 5. PMID: 27211547; PMCID: PMC4856795).
Sergeant, N., Bombois, S., Ghestem, A., Drobecq, H., Kostanjevecki, V., Missiaen, C., Wattez, A., David, J.P., Vanmechelen, E., Sergheraert, C., Delacourte, A., 2003. Truncated beta-amyloid peptide species in pre-clinical Alzheimer's disease as new targets for the vaccination approach. J. Neurochem. 85 (6), 1581–1591. https://doi.org/10.1046/j.1471-4159.2003.01818.x (PMID: 12787077).
Sharma, A., Hill, K.E., Schwarzbauer, J.E., 2023. Extracellular matrix composition affects outgrowth of dendrites and dendritic spines on cortical neurons. Front. Cell. Neurosci. 17, 1177663. https://doi.org/10.3389/fncel.2023.1177663.
Sims, J.R., Zimmer, J.A., Evans, C.D., Lu, M., Ardayfio, P., Sparks, J., Wessels, A.M., Shcherbinin, S., Wang, H., Monkul Nery, E.S., Collins, E.C., Solomon, P., Salloway, S., Apostolova, L.G., Hansson, O., Ritchie, C., Brooks, D.A., Mintun, M., Skovronsky, D.M., TRAILBLAZER-ALZ 2 Investigators, 2023. Donanemab in early symptomatic Alzheimer disease: the TRAILBLAZER-ALZ 2 randomized clinical trial. JAMA 330 (6), 512–527. https://doi.org/10.1001/jama.2023.13239 (PMID: 37459141; PMCID: PMC10352931).
Sisodia, S.S., Koo, E.H., Hoffman, P.N., Perry, G., Price, D.L., 1993. Identification and transport of full-length amyloid precursor proteins in rat peripheral nervous system, (1993). J. Neurosci. 13, 3136–3142. https://doi.org/10.1523/JNEUROSCI.13-07-03136.1993.
Sorg, B.A., et al., 2016. Casting a wide net: role of perineuronal nets in neural plasticity. J. Neurosci. 36 (45), 11459–11468. https://doi.org/10.1523/JNEUROSCI.2351-16.2016.
Steiner, Harald, et al., 2008. Intramembrane proteolysis by γ-secretase. J. Biol. Chem. 283 (44), 29627–29631. https://doi.org/10.1074/jbc.R800010200.
Steiner, Harald, Fukumori, Akio, Tagami, Shinji, Okochi, Masayasu, 2018. Making the final cut: pathogenic amyloid-β peptide generation by γ-secretase. Cell Stress 2, 292–310. https://doi.org/10.15698/cst2018.11.162.
Tanghe, A., Termont, A., Merchiers, P., Schilling, S., Demuth, H.U., Scrocchi, L., Van Leuven, F., Griffioen, G., Van Dooren, T., 2010. Pathological hallmarks, clinical parallels, and value for drug testing in Alzheimer's disease of the APP[V717I] London transgenic mouse model. Int. J. Alzheimers Dis. 2010, 417314. https://doi.org/10.4061/2010/417314. PMID: 20862386; PMCID: PMC2939388.
Thal, D.R., Rüb, U., Orantes, M., Braak, H., 2002. Phases of A beta-deposition in the human brain and its relevance for the development of AD. Neurology 58 (12), 1791–1800. https://doi.org/10.1212/wnl.58.12.1791 (PMID: 12084879).
Van Der Kolk, N., Schmitz, C., Bayer, T., Steinbusch, H., Schafer, S., Rutten, B., Van Zandvoort, M., 2005. Age-related loss of synaptophysin immunoreactive presynaptic boutons within the hippocampus of APP751SL, PS1M146L, and APP751SL/PS1M146L transgenic mice. Am. J. Pathol. 167 1. https://doi.org/10.1016/S0002-9440(10)62963-X (PMID: 15972962; PMCID: PMC1603440).
Wall, J., Donovan, K., Rosay, M., Michael, B., Silvers, R., Can, T., Colvin, M., Ni, Q., Griffin, R., Sergeyev, I., & Linse, S. Atomic Resolution structure of monomorphic Aβ42 amyloid fibrils. J. Am. Chem. Soc. 2016; 138 30. doi: https://doi.org/10.1021/jacs.6b05129. (Epub 2016 Jul 14. PMID: 27355699; PMCID: PMC5389415).
Webers, A., Heneka, M., Gleeson, P., 2020. The role of innate immune responses and neuroinflammation in amyloid accumulation and progression of Alzheimer's disease. Immunol. Cell Biol. 98. https://doi.org/10.1111/imcb.12301.
Weng, S.S.H., et al., 2019. Sensitive determination of proteolytic proteoforms in limited microscale proteome samples. Mol. Cell. Proteomics 18 (11), 2335–2347. https://doi.org/10.1074/mcp.TIR119.001560 (Epub 2019 Aug 30. PMID: 31471496; PMCID: PMC6823850).
Wildburger, N.C., Esparza, T.J., LeDuc, R.D., et al., 2017. Diversity of amyloid-beta Proteoforms in the Alzheimer's disease brain. Sci. Rep. 7, 9520. https://doi.org/10.1038/s41598-017-10422-x.
Wiltfang, J., Esselmann, H., Cupers, P., Neumann, M., Kretzschmar, H., Beyermann, M., Schleuder, D., Jahn, H., Rüther, E., Kornhuber, J., Annaert, W., De Strooper, B., Saftig, P., 2001. Elevation of beta-amyloid peptide 2-42 in sporadic and familial Alzheimer's disease and its generation in PS1 knockout cells. J. Biol. Chem. 276 (46), 42645–42657. https://doi.org/10.1074/jbc.M102790200 (Epub 2001 Aug 28. PMID: 11526104).
Wirths, Oliver, Zampar, Silvia, 2019. Emerging roles of N- and C-terminally truncated aβ species in Alzheimer's disease. Expert Opin. Ther. Targets 23. https://doi.org/10.1080/14728222.2019.1702972.
Xiong, K., Clough, R., Luo, X., Struble, R., Li, Y., Yan, X., 2007. [3H]-L-685,458 as a radiotracer that maps gamma-secretase complex in the rat brain: relevance to Abeta genesis and presence of active presenilin-1 components. Brain Res. 1157, 81–91.
Xu, C., Dong, C., Zhao, L., 2022. A review of application of Aβ42/40 ratio in diagnosis and prognosis of Alzheimer's disease. J. Alzheimer's Dis 90. https://doi.org/10.3233/JAD-220673 (PMID: 36155521).
Yamada, H., et al., 1997. The brain chondroitin sulfate proteoglycan brevican associates with astrocytes ensheathing cerebellar glomeruli and inhibits neurite outgrowth

from granule neurons. J. Neurosci. 17 (20), 7784–7795. https://doi.org/10.1523/JNEUROSCI.17-20-07784.1997. PMID: 9315899; PMCID: PMC6793916.
Yang, J., Wang, Z., Cai, H., Yuan, L., Hu, M., Wu, M., Qi, J., 2018. Sex differences in neuropathology and cognitive behavior in APP/PS1/tau triple-transgenic mouse model of Alzheimer's disease. Neurosci. Bull. 34, 736–746. https://doi.org/10.1007/s12264-018-0268-9.
Zhang, H., Wei, W., Zhao, M., Ma, L., Jiang, X., Pei, H., Cao, Y., Li, H., 2021. Interaction between aβ and tau in the pathogenesis of Alzheimer's disease. Int. J. Biol. Sci. 17 (9), 2181–2192. https://doi.org/10.7150/ijbs.57078. PMID: 34239348; PMCID: PMC8241728.
Zhang, Y., Wang, J., Zhang, Z., Su, Q., Guo, J., 2022. The relationship between amyloid-beta and brain capillary endothelial cells in Alzheimer's disease. Neural Regen. Res. 17, 2355–2363. https://doi.org/10.4103/1673-5374.335829.
Zott, B., Simon, M.M., Hong, W., Unger, F., Chen-Engerer, H.J., Frosch, M.P., Sakmann, B., Walsh, D.M., Konnerth, A., 2019. A vicious cycle of β amyloid-dependent neuronal hyperactivation. Science 365 (6453), 559–565. https://doi.org/10.1126/science.aay0198. PMID: 31395777; PMCID: PMC6690382.

Glossary

5xFAD: Mouse model with 5 familial Alzheimer's disease mutations
Aβ: Amyloid beta; peptide produced by cleavage of APP, associated with plaques in AD
Aβ x-40/42 or 1-x: Variants of amyloid beta peptides with different lengths, either N-terminally or C-terminally truncated
AD: Alzheimer's Disease
ADAMTS4: A disintegrin and metalloproteinase with thrombospondin motifs 4; ECM-modifying enzyme
AMPA: α-amino-3-hydroxy-5-methyl-4-isoxazolepropionic acid receptor; ionotropic glutamate receptor
ANOVA: Analysis of Variance; statistical test
APP: Amyloid precursor protein
APP/Ld model: Mouse model with the London mutation in the APP gene
APP/swe model: Mouse model with the Swedish mutation in the APP gene
BACE1: Beta-secretase 1; enzyme involved in the cleavage of APP to produce amyloid beta
CA1: Cornu Ammonis area 1; hippocampal subregion
CA3: Cornu Ammonis area 3; hippocampal subregion
CDK5: Cyclin-dependent kinase 5; involved in neurodegenerative pathways
Cx: Cortex
ECM: Extracellular matrix
ELISA: Enzyme-linked immunosorbent assay; used for detecting proteins
ER: Endoplasmic reticulum
FDA: U.S. Food and Drug Administration
fEPSP: Field excitatory postsynaptic potential
FL: Full-length (usually refers to full-length protein)
GAPDH: Glyceraldehyde 3-phosphate dehydrogenase; housekeeping gene/protein
GFAP: Glial fibrillary acidic protein; astrocyte marker
GSK3β: Glycogen synthase kinase 3 beta; implicated in tau phosphorylation
HAPLN1: Hyaluronan and proteoglycan link protein 1; ECM component
HC: Hippocampus
HFS: High-frequency stimulus; used to induce LTP
HUNTER: High-efficiency Undecanal-based N-termini EnRichment
Iba1: Ionized calcium-binding adapter molecule 1; marker for microglia
kDa: Kilodalton; unit of molecular weight
KO: Knock-out; gene inactivation
London mutation - V717I: Mutation in APP linked to familial Alzheimer's Disease
LTP: Long-term potentiation; synaptic plasticity mechanism
MAP2: Microtubule-associated protein 2; neuronal dendritic marker
MEA: Microelectrode array; used to record neuronal activity
ms: Millisecond
MWM: Morris Water Maze; behavioral test for spatial learning/memory
$NEX^{Cre;TG/wt}$: Transgenic mouse line with neuron-specific Cre recombinase expression
NFT: Neurofibrillary tangles; tau pathology hallmark of Alzheimer's
NMDA: N-methyl-D-aspartate receptor; glutamate receptor involved in synaptic plasticity
PNN: Perineuronal nets; ECM structures around neurons
PPR: Paired-pulse ratio; measure of synaptic presynaptic function
PSD95: Postsynaptic density protein 95; synaptic marker protein
PSEN1: Presenilin 1; part of the γ-secretase complex, associated with familial AD
ROS: Reactive oxygen species; byproducts of cellular metabolism causing oxidative stress
$ROSA26^{Mep1b\text{-}HA}$: Transgenic construct inserted in ROSA26 locus, expressing tagged Mep1b protein
sAPPα/sAPPβ: Soluble APP alpha or beta; cleavage products of APP
SDS-PAGE: Sodium dodecyl sulfate–polyacrylamide gel electrophoresis; protein separation technique
SEM: Standard error of the mean; statistical measure
SERPINA5: Serine protease inhibitor A5; associated with tau pathology
Swedish mutation - K670N/M671L: Mutation in APP associated with early-onset familial Alzheimer's Disease
Synaptophysin: Presynaptic vesicle protein; marker for synapses
TMT: Tandem mass tags; used in quantitative proteomics
wt: Wild-type